FLORIDA STATE UNIVERSITY

COLLEGE OF ARTS AND SCIENCES

STRUCTURAL EVOLUTION OF AD DAMM SHEAR ZONE, WESTERN SAUDI ARABIAN MARGIN AND ITS RELATION TO RED SEA RIFT SYSTEM

By

ABDULAZIZ SAMKARI

A Thesis submitted to the
Department of Earth, Ocean, and Atmospheric Science
in partial fulfillment of the
requirements for the degree of
Master of Science

2015

Abdulaziz Samkari defended this thesis on November 12, 2015.
The members of the supervisory committee were:

David W. Farris
Professor Directing Thesis

James F. Tull
Committee Member

Leroy A. Odom
Committee Member

The Graduate School has verified and approved the above-named committee members, and certifies that the thesis has been approved in accordance with university requirements.

ACKNOWLEDGMENTS

First and foremost, I would like to thank Allah “God” for everything, for providing me his blessing to accomplish this thesis and made me who I am today. I will forever be thankful to my advisor Dr. David Farris, my thesis advisor, for his patience, support, feedback and inspiration. I’m forever thankful not only for his support but also to encourage me throughout my academic program. I have never expected to learn a lot of techniques and skills not only in the field of structural geology but also in geochemistry and other subdisciplines. He and the other committee members, Dr. James Tull, and Dr. Leroy Odom, guided me throughout this process. This thesis couldn’t have been written without their supervision. A special thanks to Dr. Haitham Baggazi for being my external advisor back in King Abdulaziz University. The field trip could not have been accomplished without his assistance.

Most importantly, I’m forever grateful to my family for their spiritual and financial support. Their kindness made me focus and overcome during the past two years. I am also thankful for having wonderful colleagues and class-mates who have helped me a lot during this years.

I would like thank the government of Saudi Arabia and King Abdulaziz University for giving me the opportunity to study abroad and obtain my master degree. I am lucky to have a strong scholarship funded by the ministry of higher education and King Abdulaziz University.

Last but not least, although only my name is written on the cover page of my thesis project, many people have participated in this scientific journey and contributed in this project. I owe you all.

TABLE OF CONTENTS

LIST OF TABLES

LIST OF FIGURES

.

ABSTRACT

This project seeks to determine how the opening of the Red Sea rift was influenced by pre-existing tectonic features and to place constraints on the structural evolution of the western Saudi Arabia margin. In detail, we investigate whether or not the Ad Damm Shear Zone (ADSZ) was solely a Neoproterozoic structure or if it has been reactivated during the Cenozoic. The Ad Damm shear zone is a major mylonitic right-lateral structure that bounds the Jeddah terrane to the north from the Asir terrane to the south.

South of the ADSZ, the Red sea rift exhibits well-developed linear magnetic anomalies, but north of it, they are not present. On land, the ADSZ bounds a large topographic escarpment perpendicular to the rift margin, with higher elevations to the south. In addition, recent studies show active seismicity within the Jeddah terrane bounded by the ADSZ. These observations collectively suggest some type of tectonic reactivation.

Four techniques were used to test this hypothesis: field mapping, satellite image processing (ASTER, SPOT-5), microstructural studies, and whole rock geochemistry. Field observations show various meta-plutonic and volcanic rocks that range in age from 800-540 Ma. North of the ADSZ, Jeddah terrane is characterized by heterogeneous magmatism with extensive meta-basalt intruded by silicic plutons of varying size. South of the ADSZ, Asir terrane is characterized by larger-scale granitic batholiths. In addition, a large synform, likely a km-scale drag fold, is present along the northern edge of the ADSZ. Felsic dikes intrude a package of metabasalt and are folded in the synform. A younger generation of Eocene to Miocene basaltic dikes cut the mylonitic shear zone at a high angle.

Petrographic analyses of mylonitic rocks indicate dynamic recrystallization and grain size reduction suggesting high-temperature recrystallization. Field observations also found a lack of low temperature fault zone rocks (e.g. gouge) except for isolated brittle slickensides. Spider

diagram of Jeddah, Asir terranes, and ADSZ rocks are characterized by an arc- related signature, which related to the amalgamation of Jeddah and Asir terranes and defined ADSZ as Neoproterozoic structure. In contrast, Eocene-Miocene basaltic dikes and southern basaltic flow are represented by a rift- related signature, which is associated with development of Red Sea rift system. However, differences in the crustal characteristics of Asir and Jeddah terranes still influence the ongoing tectonic evolution of the Red Sea rift.

CHAPTER 1

INTRODUCTION

1.1 Purpose of Study

For the last few decades, Saudi Arabia has experienced earthquakes recorded by 89 stations around the kingdom, and monitored by the National Center of Earthquakes and Volcanoes (Roobol and Kadi, 2008). Major historical earthquakes of the Arabian Peninsula include an earthquake with a magnitude of 7.2 in the Gulf of Aqaba in 1995, NW of Saudi Arabia; an earthquake in Dhamar (SW of the Arabian Peninsula) that killed about 1,500 people in 1982; and Jazzan (SW of Saudi Arabia) affected by an earthquake in 1941 (Coleman, 1993). In addition, the areas considered to be of highest potential risk are located along the Red Sea, and so, the main objective of this project is to better understand the opening of the Red Sea rift and to place constraints on the tectonic and structural evolution of the western Saudi Arabian margin. More specifically, the present work aims to investigate whether or not Ad Damm Shear Zone was solely Neoproterozoic structure or has been reactivated during Cenozoic.

1.2 Location

The study area, measuring a length of 50 km N-S by 80 km W-E, is located in Al Lith quadrangle, south central part of Saudi Arabia. In addition, the area is bounded by 20^{o} 45´ 00´´ to 21^{o} 15´ 00´´ N and by 39^{o} 45´ 00´´ to 40^{o} 15´ 00´´ E (Figure 1.1). Al Damm shear zone, represented by a linear zone of valleys and sheared rocks, strikes NE- SW and bounded by Harrat Rahat to the north, Red Sea to the west, Al Taif area to the north, and Harrat Hadan to the east.

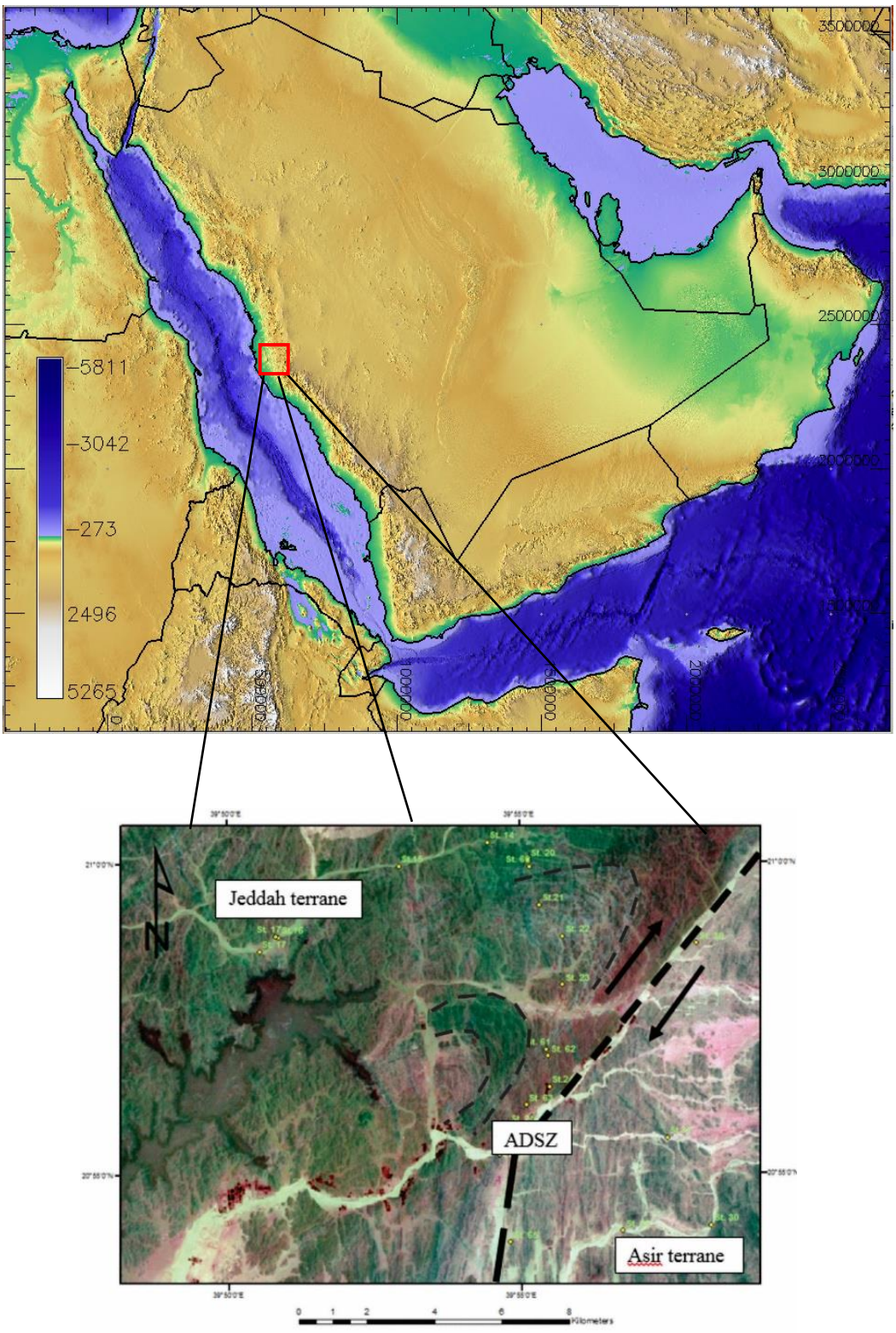

Figure 1.1 Location map of the study area.

1.3 Tectonic History

Tectonically, most of Neoproterozoic rocks are exposed on the flanks of Red Sea and recognized by the Arabian plate to the east and Nubian shield to the west (Hamimi and other, 2014). The Arabian Nubian shield is shaped by the amalgamation of different terranes, which have different geologic ages (Hamimi and other, 2014). According to Johnson (1997) the Arabian plate is divided into nine terrains which separated by faults or suture zones. Earliest terranes include Jeddah (870- 740 Ma; Kröner et al., 1993) and Asir (850- 750 Ma; Johnson and Woldehaimaot, 2003). Middle age terrane contains Midayan (780- 710 Ma; Ali et al., 2010) and younger terranes include Ar Ryan (> 670; Stoeser and Stacey, 1988) and Ad Dawadimi (674± 6; Cox, 2011). The age of the different terranes is determined based on the isotopic composition, geochronological ages, the apparent structures, as well as the lithostratigraphic variation (Johnson, 2006). The Arabian plate is composed of the Arabian shield, which is surrounded by active tectonic boundaries in all directions (Figure 1.2). To the northeast, there is a collision zone between the Arabian plate and Eurasian plate, along Zagros Mountain and Bitlis thrust system. Along the western and southern margins there is rifting and drifting of Red Sea and Gulf of Aden. Finally in the north, there is a transform plate boundary that strikes toward Dead Sea. Moreover, the Arabian plate has been subjected to two major episodes of volcanic activities due to development of Red Sea and Gulf of Aden rift system (Bohannon et al., 1989). The first episode took place during late Oligocene- early Miocene, and the second episode occurred during mid- Miocene until the current time. Both episodes involve intense volcanic eruptions and uplifting (Camp and Roobol, 1992). The oldest basalt composition associated with rifting of Red Sea is characterized by olivine transitional basalts to alkali olivine basalt (Al-Saud, 2008). Although the sea floor spreading in south of Arabian Shield is well observed through a linear

magnetic anomalies, doesn't correlate with north part of Arabian plate. The southern segment of t h e Red Sea is affected by the upwelling of Afar plume. Whereas the northern part of the Red Sea is influenced by its connection with the Dead Sea transform fault (Lazar, et al., 2012).

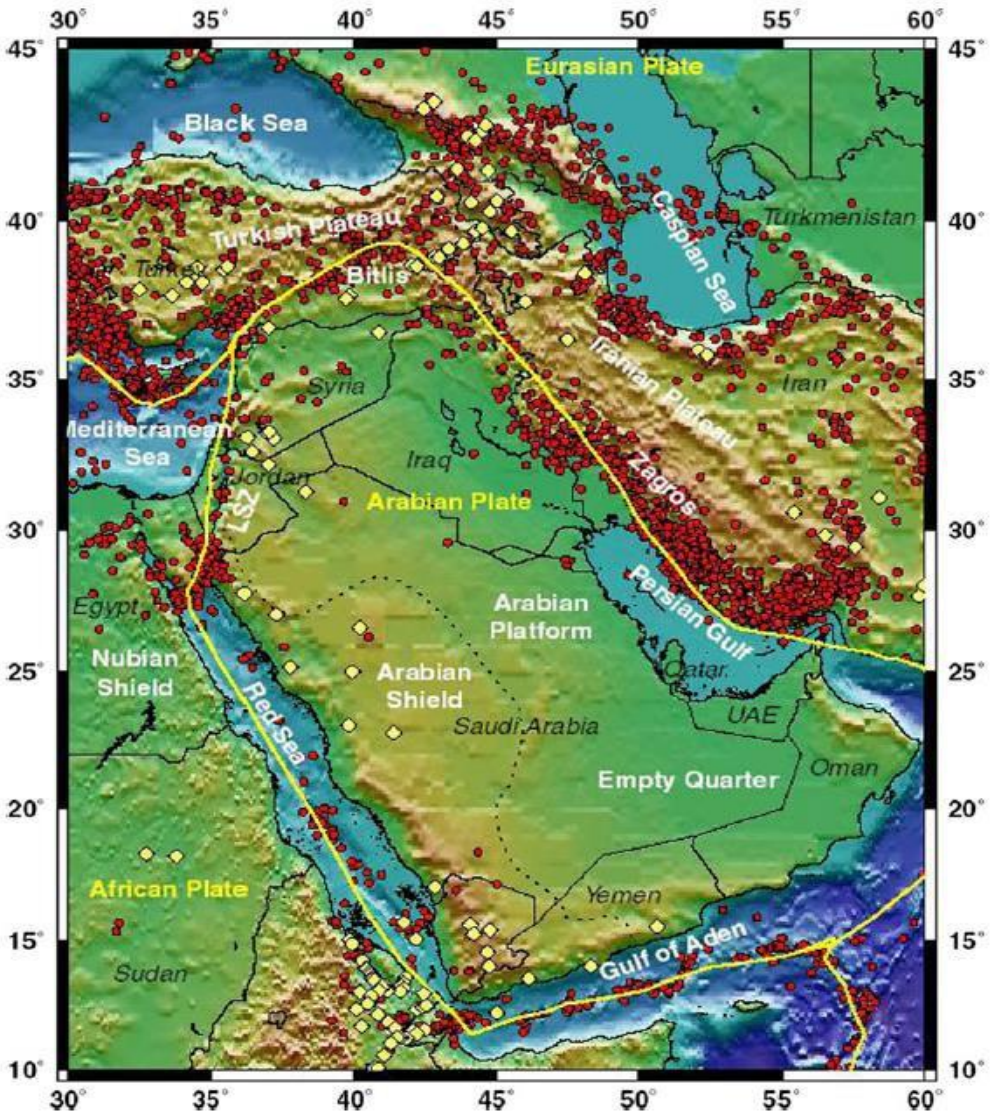

Figure 1.2 Active tectonic boundaries adjacent to Arabian shield (Roobol and Kadi, 2008).

1.4 Structural History of the Ad Damm Shear Zone

The structural setting of the investigated area is constrained by Al Damm Shear Zone, which runs across the area from northeast to southwest, and separates the area into Jeddah and Asir terrane (Al- Saud, 2008). Firstly, the southern structural part is dominated by N-S foliation surfaces and most folds and mineral lineation plunging toward the south. Secondly, the northern structural part is recognized by the northeast- trending mineral lineation. Recent studies indicate that the Al- Damm Shear Zone is a tectonic contact between Jeddah and Asir terranes, which has an age about 620- 540 Ma, determined by multiple sample Rb-Sr isochrones (Fig. 1.3) (Hamimi and other, 2014). However, crystallization age of Plutonic rocks adjacent to Ad Damm Shear zone display older ages about 800-700 Ma, using U-Pb zircon, which indicates the ADSZ rocks are significantly younger. In addition to this, Asir terrane thought to be created by the amalgamation of many terranes and characterized from other terranes by thicker granitic rock. Whereas the Jeddah terrane formed by a northward migrating SE- dipping arc (Johnson and Woldehaimanot, 2003). Hamimi and others (2014) explain the deformation history of Ad Damm Shear Zone and identified three phases of deformation. The first phase (D_1) involves the contraction between NW- SE, which led to the formation of thrust faults that strikes NE and tight- overturned folds. The second phase of deformation (D_2) encompasses a compressional regime that strikes NE- SW, results in evolution of open folds. The last phase of deformation (D_3) represented by NE- SW dextral transcurrent shear zone which led to the formation of Ad Damm Shear zone on a large scale. Likewise, the deformation history of the shear zone on the other flank of Red Sea (Nubian shield) is similar and compatible with the deformation observed in the Ad Damm Shear Zone (Fig. 2) (Hamimi and other, 2014). According to Al- Saud (2008), the investigated area has been subjected to multiple generations of faults that strike NNW-SSE,

NE- SW. Aeromagnetic data reveal small portions of magnetic bodies, which are believed to be associated with Eocene and younger Red Sea rifting process (Al- Saud, 2008). Furthermore, most of the recent faults are thought to be responsible for geographic relief differences between the northern and southern part of Jeddah. On land, the ADSZ bounds a large topographic escarpment perpendicular to the rift axis with higher elevation to the south. Also, the seismicity along Ad Damm Shear Zone and dextral lateral focal mechanism solutions are one of the significant evidence that indicate some types of reactivation (Al- Saud, 2008). Thus, this project aims to investigate whether or not ADSZ is Neoproterozoic structure or has been reactivated during Cenozoic.

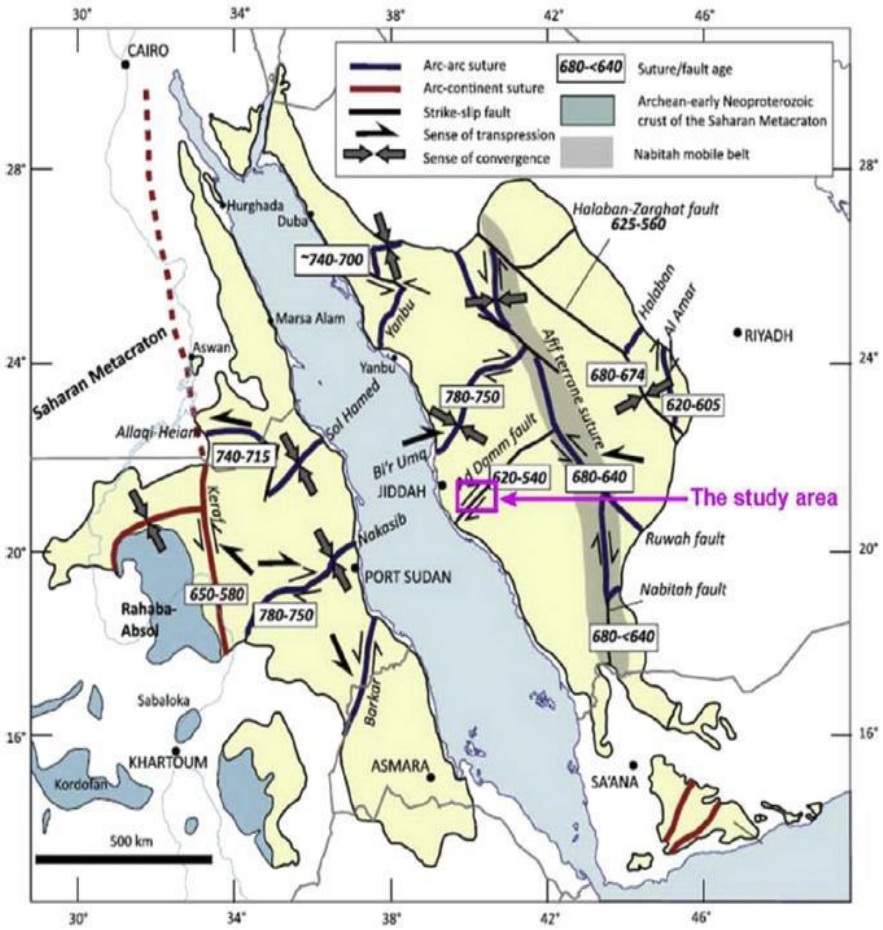

Figure 1.3 Tectonic map of the Arabian Nubian shield, displaying the ages of several terranes (After Johnson et al., 2011).

1.5 Regional Geology of the Study Area

Geologically, the ancient rocks in the Al- Damm Shear Zone area are comprised of Neoproterozoic basement which includes mostly of plutonic rocks of various sorts with amphibolitic host rock. (Al- Saud, 2008). The original units in this area before deformation were igneous rocks mainly diorite, granite and volcano-sedimentary rocks, dissected by dike swarms of diverse ages and composition. Five types of intruded lava are observed and recognized as Sharqah, Milh, Ju'ranah, Hashafat and Nu'man complex body (Moore and Al-Rehaili, 1989). Ju'ranah complex is located in the northwest of Makkah batholith and composed mainly of granodiorite and tonalite.

In Jeddah terrane, the Milh intrusion body is characterized by a weak foliation, and is comprised of metadiorite, gabbro and tonalite (Al-Saud, 2008). In Asir terrane, Nu'man complex can be identified as a huge intrusion body, located in the SSE of the study area and extends toward Ta'if area in the north (Al-Saud, 2008). It is comprised mostly of granite gneiss and is believed to be a syntectonic intrusion during the deformation of the volcanic and the sedimentary rocks (Figure 1.4) (Johnson 1997). Other studies show the age of the sheared granite from Nu'man intrusion (542± 23) using Rb- Sr isochron (Fleck and Hadley, 1982). However, Johnson (2006) suggests that the determined Rb-Sr age represents cooling age rather than the crystallization age.

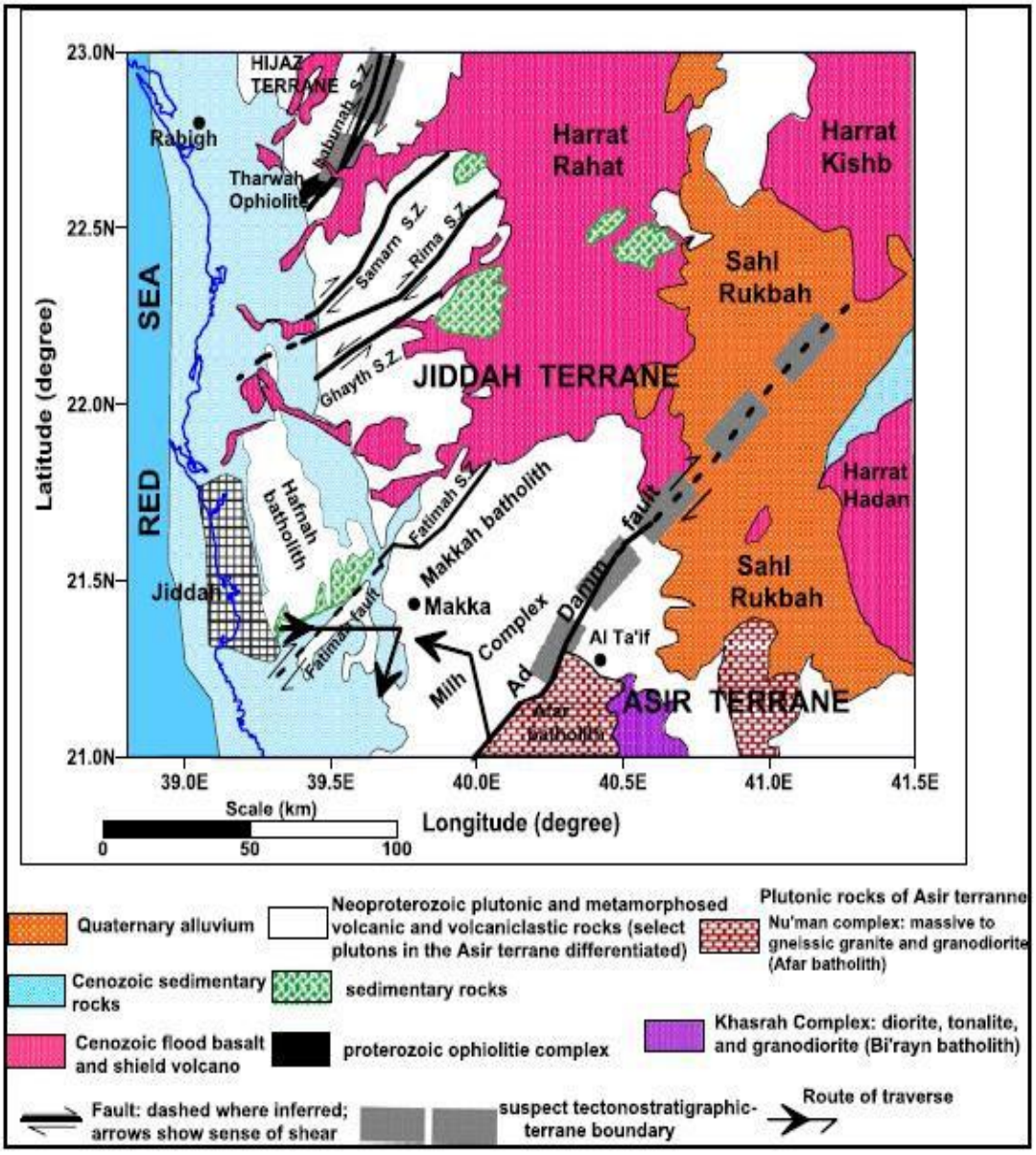

Figure 1.4 Geologic map of Ad- Damm Shear Zone, emphasizing the different geologic rock units (After Johnson, 1997).

CHAPTER 2

ANALYTICAL METHODS AND RESULTS

2.1 Field Observation

First, field investigation was carried out in order to define:

1- The relation between the structural elements, lithologic characteristics, and kinematic indicators in the studied area.
2- The structural evolution of the studied area and its relation to the adjacent rock unites.

Pre-field work was carried out to prepare the necessary geologic maps as well as the satellite images. This step is mandatory for site investigation. The preparation of geologic maps and satellite images require certain types of geologic software to process and digitize the potential locations within the study area. During field work, rock samples and structural data were collected from 69 stations (table 2.1) (Figure 2.1). In addition, many traverses and transects were selected and outlined from west to east and from northwest to southeast.

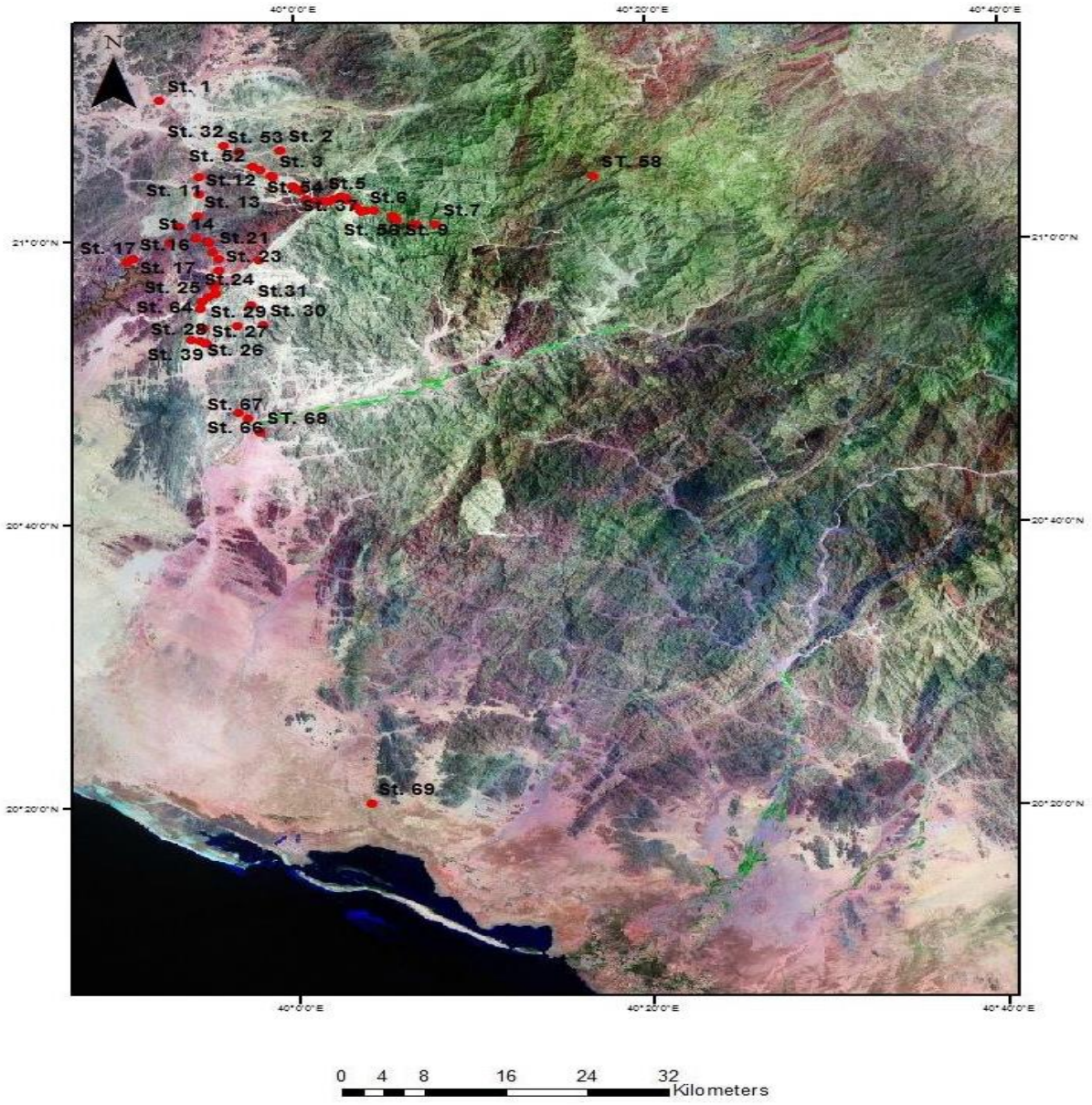

Figure 2.1 Mr-SID image shows the location of field stations.

Table 2.1 Field data set.

St. No	Apparent Structure	Strike	Dip	Trend	Plunge	Fault Plane (Strike/Dip)	Slickenline (Plunge/Trend)	Rake Angle
4	Foliation (Mylonite Zone)	079	43					
4	Revers Left Lateral Strike Slip Fault	075	40					52
5	Foliation (Light Blue, Pinkish Granite)	110	59					
7	Foliated Granite	334	83					
9	Dexteral Normal Fault	270	70					20
10	Foliated Granite	330	42					
10	Fructure Plane	072	81					
12	Foliated Gabbro	304	80					
13	Foliated Green Schist	000	90					
14	Foliated Granite	150	60					
15	Foliated Granite	085	25					
17	Foliated Surface	182	54					
17	Fault Plane (Revers Fault)	222	69				69/305	
17	Foliated Surface	025	48					
18	Foliated Surface	238	50					
18	Foliated Surface	225	48					
18	Fracture Surface	005	19					
20	Revers Fault	185	59				59/077	
20	Foliated Surface (Mica, Felsic Granite)	059	65					
20	Foliated Surface (Mica, Felsic Granite)	205	65					
20	Foliated Surface (Mica, Felsic Granite)	018	59					
20	Foliated Oriented Sample	130	70					
20	Meniral Leniation			050	70			
20	Foliated Surface	219	62					
20	Foliated Surface	195	77					
21	Foliated Schist	195	15					
22	Intersection Leaniation			030	45			
22	Meniral Leniation			020	45			
22	Foliated Green Schist	330	50					
23	Foliated Green Schist	025	53					
23	Foliated Green Schist	025	55					
23	Foliated Green Schist	047	60					
23	Foliated Green Schist	065	54					
24	Shear Zone (Foliation)	015	50					
24	Shear Zone (Foliation)	235	50					
25	Hingin Zone			015	40			
25	Foliation	214	70					
27	Fold Axis			015	32			
27	Foliation	000	77					
27	Tight Fold Axis			000	18			
29	Meniral Leniation			010	18			
29	Dikes	N-S						
29	Foliated Surface	005	55					
31	Thrusted Granite	340	15					
31	Thrusted Granite	225	10					
31	Right-Thrusted Granite						10/005	
31	Right-Thrusted Granite						10/002	
34	Left_lateral-Revese Fault					000/44		23
35	Mylonitic Granite Foliation	154	35					

Table 2.1 Continued.

St. No.	Apparent Structure	Strike	Dip	Trend	Plunge	Fault Plane (Strike/Dip)	Slickenline (Plunge/Trend)	Rake_Angle
38	High Ductile Strain Granite_Foliation	085	65					
38	Mineral Lineation			005	05			
38	Foliation	005	65					
38	Foliation	018	60					
39	Foliation	010	70					
40	Foliation	098	88					
40	Mineral Lineation			125	60			
41	Mineral Lineation			275	62			
42	Sheared Granite Foliation	298	65					
42	Mineral Lineation			085	10			
42	Normal Fault Plane					016/30		
42	Right- Lateral Fault Plane					090/38	32/075	
43	Foliation	085	60					
44	Foliation	245	33					
44	Foliation	250	34					
45	Foliation	190	80					
46	Basaltic Dike-Granite Contact	130	70					
46	Foliation	218	65					
46	Mineral Lineation			234	25			
47	Foliation	035	80					
47	Mineral Lineation			034	23			
49	Basaltic Dike-Granite Contact	030	70					
50	Foliation	135	76					
50	Foliation	155	70					
52	Foliation	110	67					
54	Foliation	209	88					
54	Foliation	211	82					
55	Foliation	215	75					
55	Mineral Lineation			190	07			
56	Foliation	340	78					
57	Foliation	210	78					
57	Mineral Lineation			205	72			
58	Foliation	230	64					
58	Mineral Lineation			235	80			
59	Foliation	230	70					
61	Felsic Dikes	060	78					
62	Felsic Dikes	227	53					
62	Felsic Dikes	214	62					
62	Felsic Dikes	220	80					
62	Right-Lateral Strike silp Fault					224/80		
63	Mineral Lineation			214	12			
64	Foliation	190	78					
67	Foliation	352	75					
67	Foliation	354	80					
67	Mineral Lineation			356	12			
68	Foliation	353	78					

The large-scale structure of the Ad Damm Shear Zone (ADSZ) is dominated by right-lateral strike-slip ductile mylonitic shear zone that strikes NE-SW and separates between the Asir and Jeddah terranes (Al- Saud, 2008). Field work was carried out to simplify the different geologic units and to reconstruct the geologic history of the investigated area. According to geochronological-data, the study area can be divided into five main geologic units: Jeddah terrane (ca. 870- 740 Ma; KrÖner et al., 1993), Asir terrane (850- 750 Ma; Johnson and Woldehaimaot, 2003), ADSZ rocks (ca. 620-540; Hamimi et al., 2014), Eocene-Miocene Ad Damm dikes complex and southern basaltic flow (Camp and Roobol, 1992). The geological map and cross-section were constructed using interpretation of satellite imagery, field observations, structural measurements, geochronological data, and lithostratigraphic differences (Figure 2.2).

A traverse was carried out from NW (Jeddah terrane) –SE (Asir terrane) and major rock units are Gabbro, Migmatite, Granite, Gneiss Granite and amphibolite truncated by numbers of basaltic dikes. Sense of shear has been identified in many locations such as station 2 and 5 and measured as right-lateral strike-slip fault (Figure 2.3). Another traverse was also carried out from NE (Asir Terrane) to SW (Jeddah terrane), and indicates significant geologic similarities between rock units at different points along the ADSZ. ADSZ rocks were defined primarily by linear structures and mylonitic fabrics on granitoid bodies. Brittle small-scale of normal faults have also been observed (see station 13) and, strikes N-NW. Such normal faults may be associated with Red Sea Coastal Plain Faults (Figure 2.4).

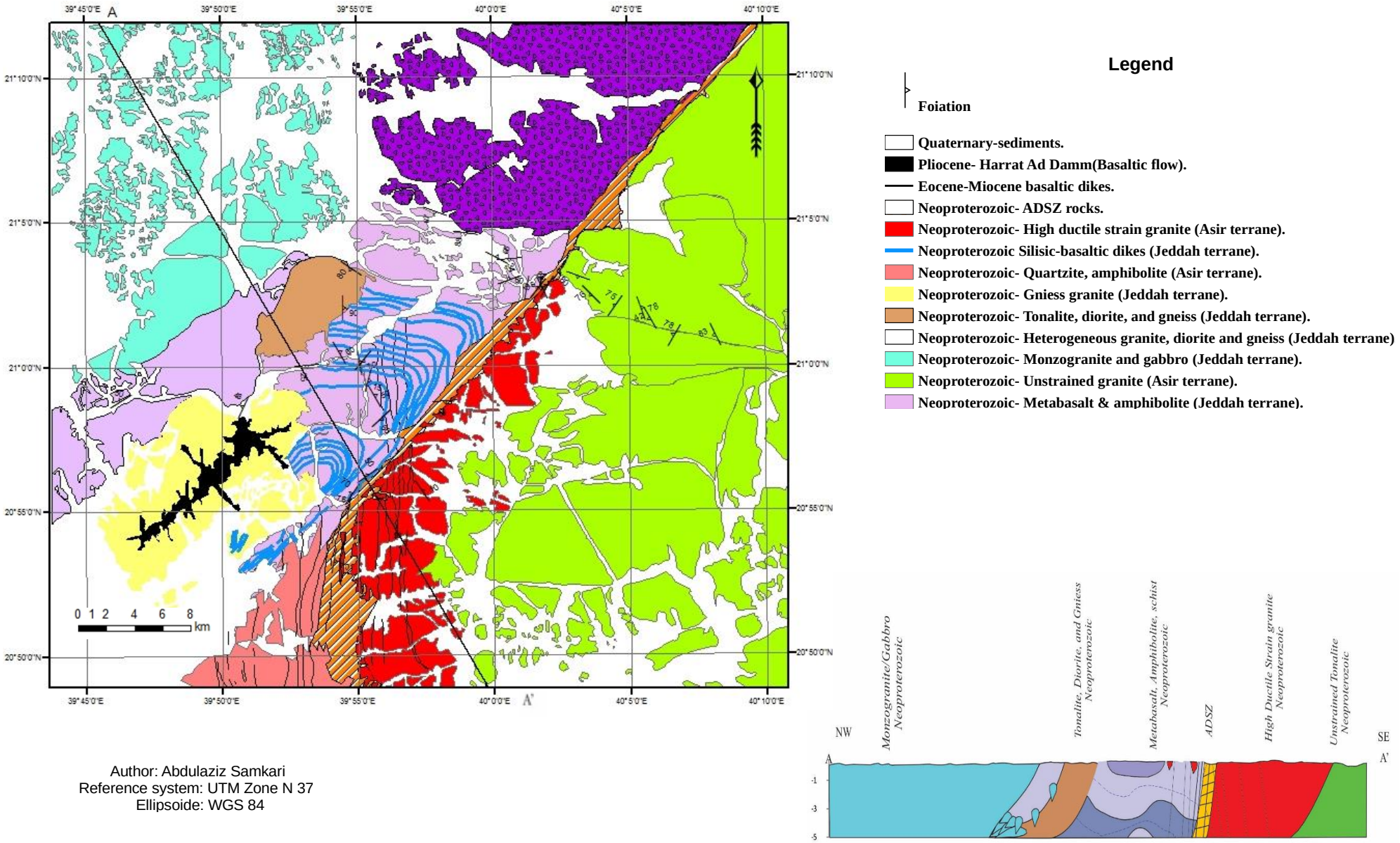

Author: Abdulaziz Samkari
Reference system: UTM Zone N 37
Ellipsoide: WGS 84

Figure 2.2 Geological map and cross-section of the study area.

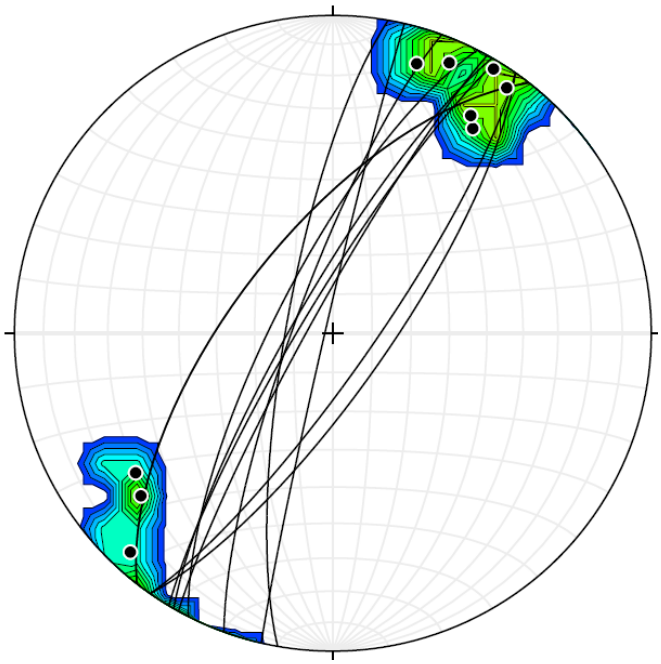

Figure 2.3 displays foliation and mineral lineation in the ADSZ

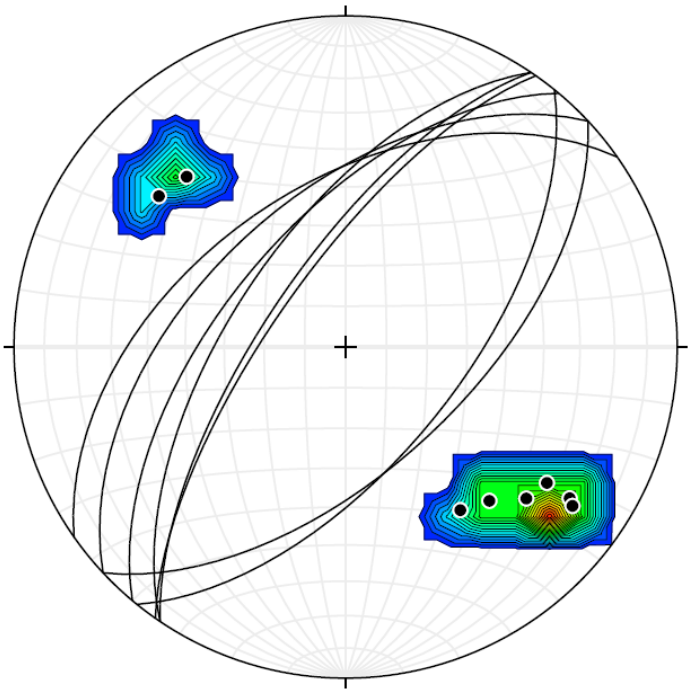

Figure 2.4 Foliation data of Synform drag fold in Jeddah Terrane.

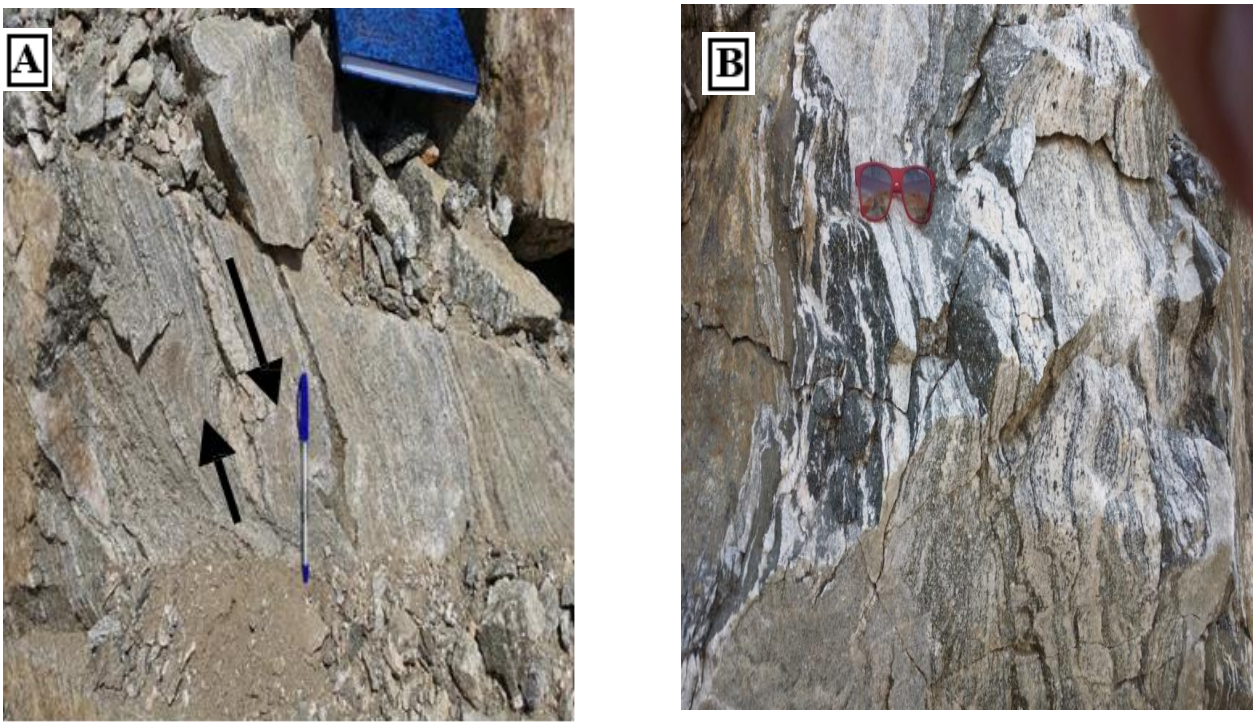

Figure 2.5 (A) Show the sense of movement (St. 2), (B) dispalys pegmatitic texture (St. 2)

Figure 2.6 (A) Shows normal movement (St. 13), (B) displays mylonitic fabrics of ADSZ rocks (St. 47).

2.1.1 Jeddah Terrane

The structural measurements indicate that the Jeddah terrane is characterized by NE-striking foliation located at synform drag folds, and its lithology is defined by heterogeneous magmatism. The major geologic units are amphibolite and meta-basalt intruded by silicic plutons with different sizes. Moreover, the most prominent structural feature in the Jeddah terrane, is the km-scale synform drag folds which is located at the edge of ADSZ. The large-scale synform drag fold contains meta-basalt and amphibolite units, intruded by number of felsic dikes (Figure 2.5). These rock units are then folded and cut by younger group of Eocene-Miocene basaltic dikes at high angle. In addition, sense of shear has been carefully identified in many locations such as station 2, 5, 21 and measured as right-lateral strike-slip fault (Figure 2.3). Finally, several normal faults have been located in station 13, which strike N-NW may be associated with Red Sea Coastal Plain Faults (Figure 2.4).

2.1.2 Asir Terrane

The structural geometry of the Asir terrane is generally dominated by NE to NWstriking foliation and the lithological units are defined as large-scale granitic batholiths that includes granodiorite, diorite and granite, which intruded by number of Eocene-Miocene basaltic dikes. Field observations reveal that the intensity of the foliation increases towards ADSZ and conversely dies out away from the shear zone (Figure 2.6). The sense of shear also shows dextral displacement. The magnetic susceptibility was measured and it is relatively low comparing to Jeddah terrane, which could be related to the amount of basaltic dikes intruded within the host rock of Jeddah terrane. Along the edge of ADSZ and Asir terrane, high ductile strain granite was recorded which indicate high pressure-temperature during shearing.

Figure 2.7 Shows the host rock (amphibolite) cut across by number of felsic in the large Jeddah terrane drag fold (St.60).

Figure 2.8 Shows the unstrained granite from the Asir terrane (St. 57).

2.1.3 Eocene-Miocene Basaltic Dikes

The intrusion of the Eocene-Miocene basaltic dikes are associated with development of Red sea rift system (Camp and Roobol, 1992). Most of the intruded dikes comes from harrat Ad Damm and harrat Tahat and have age about 11 Ma (Camp and Roobol, 1992). These dikes are cut-cross Asir and Jeddah terranes at relatively high angle suggesting that they are post tectonics features (Figure 2.5).

Figure 2.9 Eocene-Miocene basaltic dikes intruded within ADSZ rock unit (St. 39).

2.1.4 Ad Damm Shear Zone Rock Unit

ADSZ is a right-lateral strike-slip mylonitic zone, which forms the boundary between the Jeddah and Asir Terrane, and has NE-SW strike. Field data illustrates that ADSZ bounds Jeddah terrane to north and Asir terrane to south. Lithologically, the rock units are mainly sheared mylonitic granites, located on both sides of ADSZ- due to the ductile deformation during shearing process. Structurally, the field relation shows that the mylonitic fabrics are cut by the recent Eocene-Miocene basaltic dikes at relatively high angle (Figure 2.7). In addition, Orientation of foliation and the trend of mineral lineation are parallel to the orientation of ADSZ (NE-SW) and therefore reflect the re-orientation and recrystallization of minerals during shearing.

2.1.5 Southern Basalt Flow

The southern basaltic flow located locally south in the investigated area (Figure 2.8) is related to development of the opening of Red Sea underneath the Arabian plate (Al- Saud, 2008). It is considered to be the youngest rock units exposed in the study area (2 Ma; Coleman, 1993).

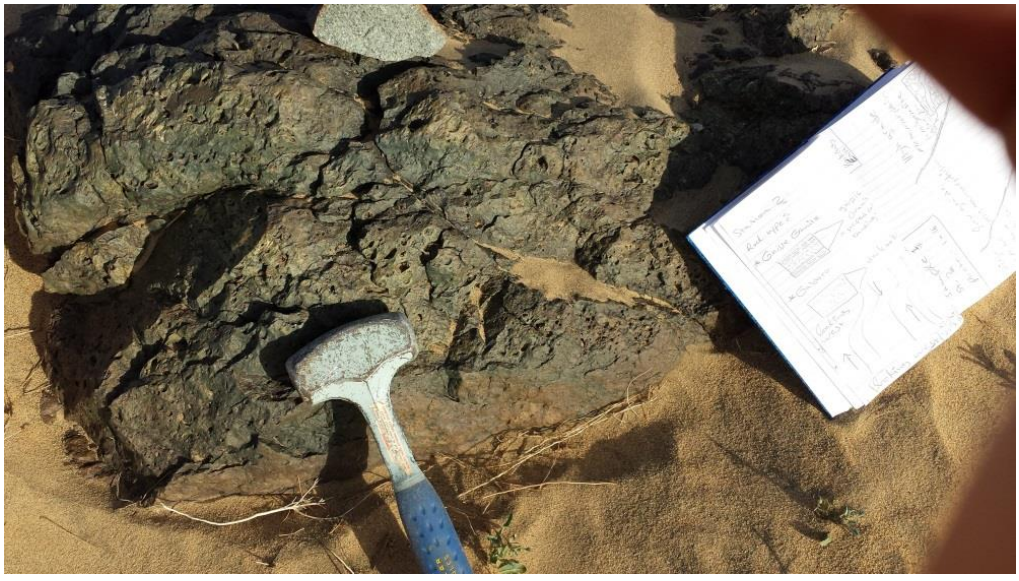

Figure 2.10 Southern basaltic flow of (St. 69).

2.2 Satellite Image Processing

Second, satellite image processing is an important tool for field mapping and geologic interpretation. It provides valuable information for navigation and to locate potential outcrops (Sabins, 1999). Four image analysis software packages have been used to process and layout the different satellite images. These programs are Arc map, ENVI, ERDAS and Global Mapper (Figure 2.9). The multiple bands within the satellites imagery help to interpret wavelengths of light that can't be seen by naked eye (Pour and Hashim, 2011). During pre- field work, several satellite images with different resolutions- ASTER (advanced spaceborne thermal emission and reflection radiometer), Mr-sid (multiresolution seamless image database) and SPOT_5 (Satellite Pour l'Observation de la Terre). ASTER image is a useful tool for mineralization (Sabins, 1999), whereas, Mr- SID is being used as navigation for tracking due to its large coverage (Shand, 2002). SPOT- 5 can be utilized to pick and detect the different structural components and geologic units due to its high resolution (Pasqualini et al, 2005) (Figure 2.10). Image processing for ASTER and SPOT- 5 raw data involve three main steps. Firstly, layer stacking the satellite image using ENVI software. Secondly, mosaicking the two scenes can be made using INVI or ERDAS Imaging software. Finally, decorrelation stretch is being used to improve color discriminations of a satellite image with a significant band to band correlation and hence easy to interpret (Dong, 2003).Yet, this process is normally applied to RGB three band images using ENVI or ERDAS software. So it is mandatory to follow the two first steps before starting the decorrelation stretch. On the other hand, Mr- SID does not require the three previous instructions. It contains a compressed large raster image that can be quickly viewed due to its small size comparing to ASTER and SPOT- 5 (Shand, 2002). Hence, it can be utilized as navigation map in the field using global mapper software. All the satellite images are geo-

referenced using the universal transverse Mercator (UTM) and projected using WGS 84 (World Geodetic System Ellipsoid).

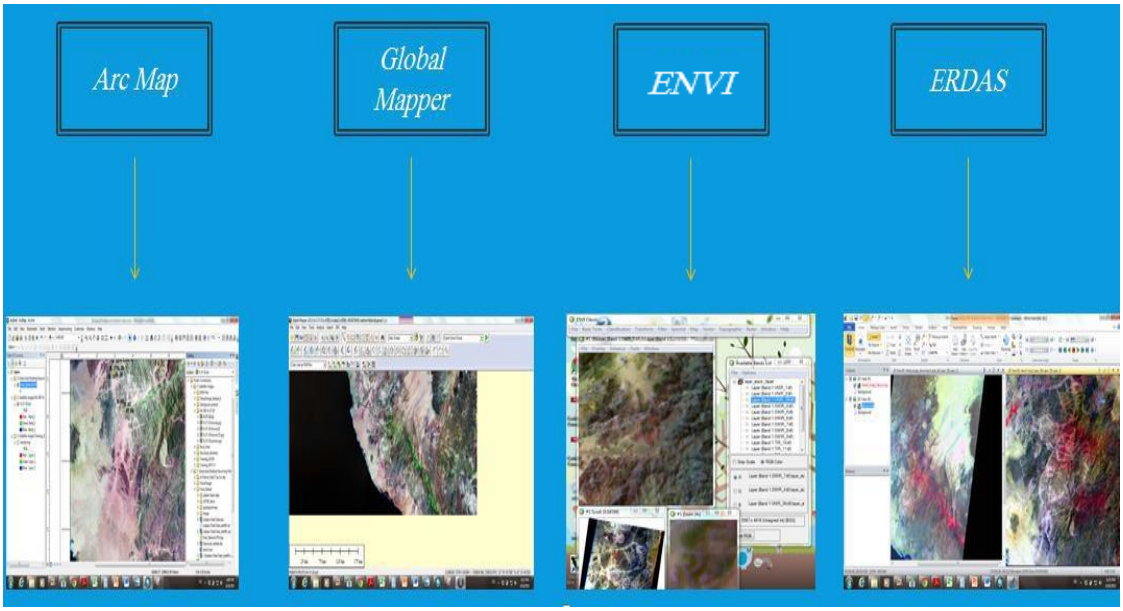

Figure 2.11 Shows several remote sensing programs that were used in this research project.

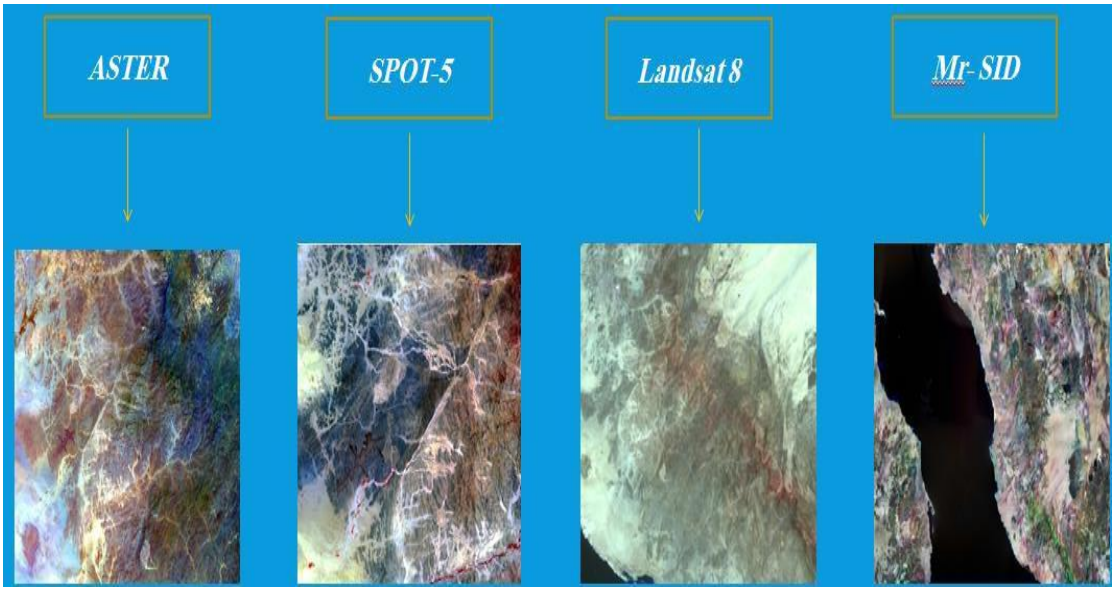

Figure 2.12 Displays several satellite images that were used in this research project.

In detail, the Mr-SID image was uploaded on to the global mapper software as a navigation based map, during the field mapping, due to its high coverage (Figure 2.11).

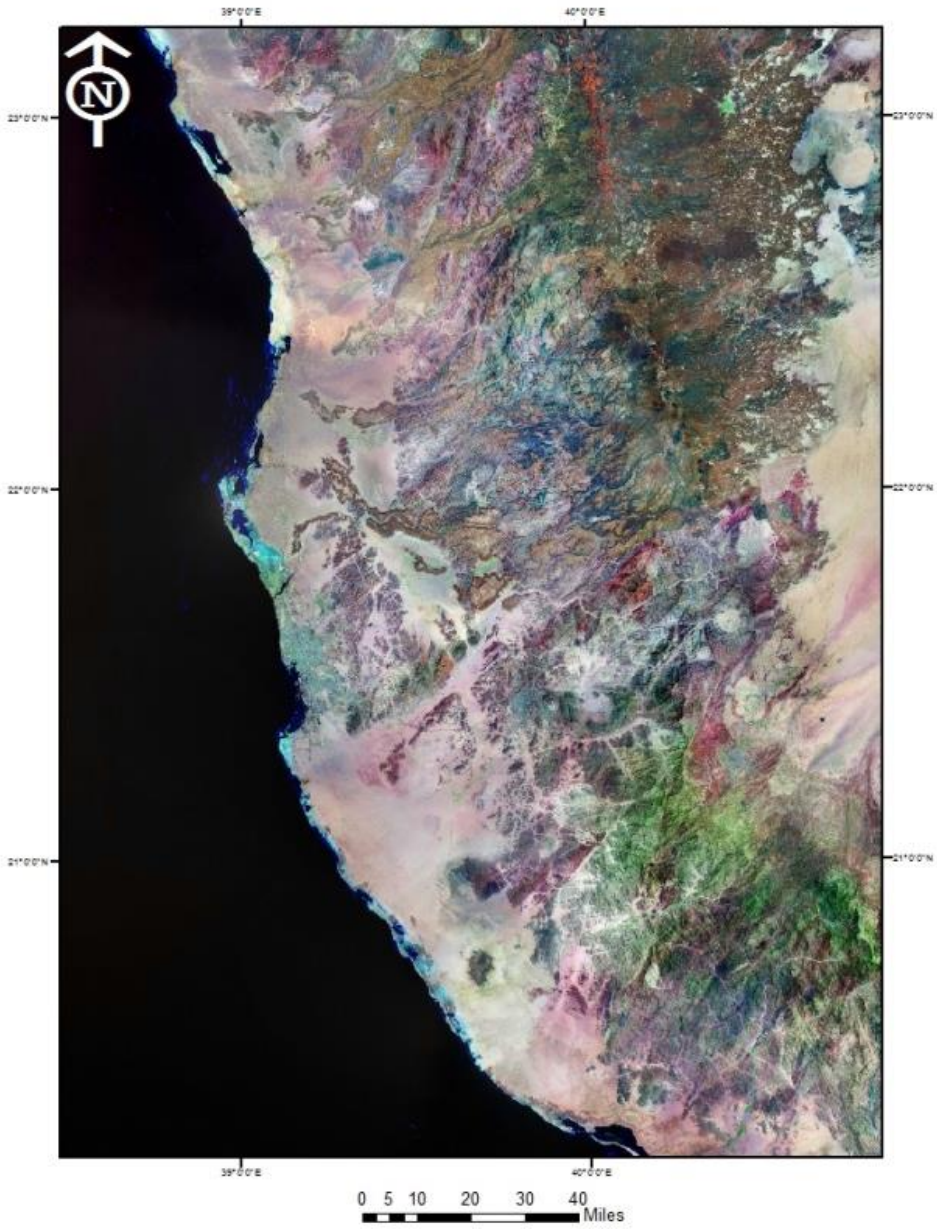

Figure 2.13 Mr-SID image covers the western-central part of the Arabian Shield.

ASTER data, when integrated with field mapping, proved to be best at differencing the major lithologic units. The decorrelation stretch technique was applied, using the ERDAS software, to enhance differences in the color by stretching the image pixels. Hence, it improves the ability to detect and separate the different geologic units (Figure 2.12).

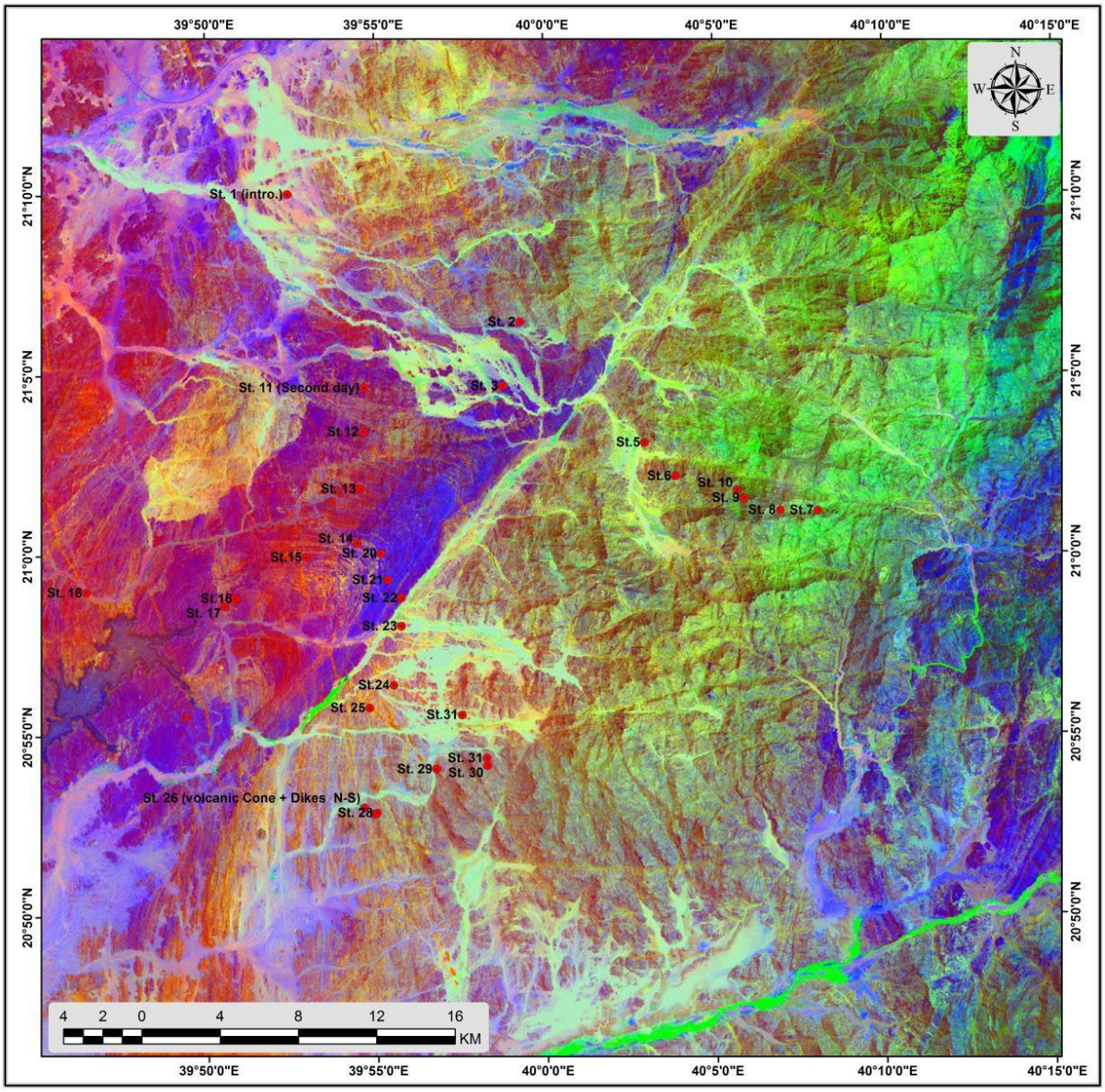

Figure 2.14 ASTER image using decorrelation stretch technique.

The Ad Damm linear valley and other minor valleys are well defined in white color. While the dark blue color represents amphibolite and metabasalt at the edge of Jeddah terrane and ADSZ. The dull green color displays the unstrained granite (Asir terrane) and the reddish brown color symbolizes Jeddah terrane (heterogeneous granite). Harrat Ad Damm is clearly demonstrated in black color. Landsat 8 is used, for the same purpose as ASTER, to separate and distinguish the different geologic units.

SPOT-5 is characterized by its high resolution (2.5m). Hence, it can be utilized to detect the different geologic structure (Figure 3.5). The synform drag fold is well-observed in the SPOT-5 image and drag fold can be seen to be cut by a group of basaltic dikes. The sense of movement along ADSZ is clearly defined and shows a dextral displacement.

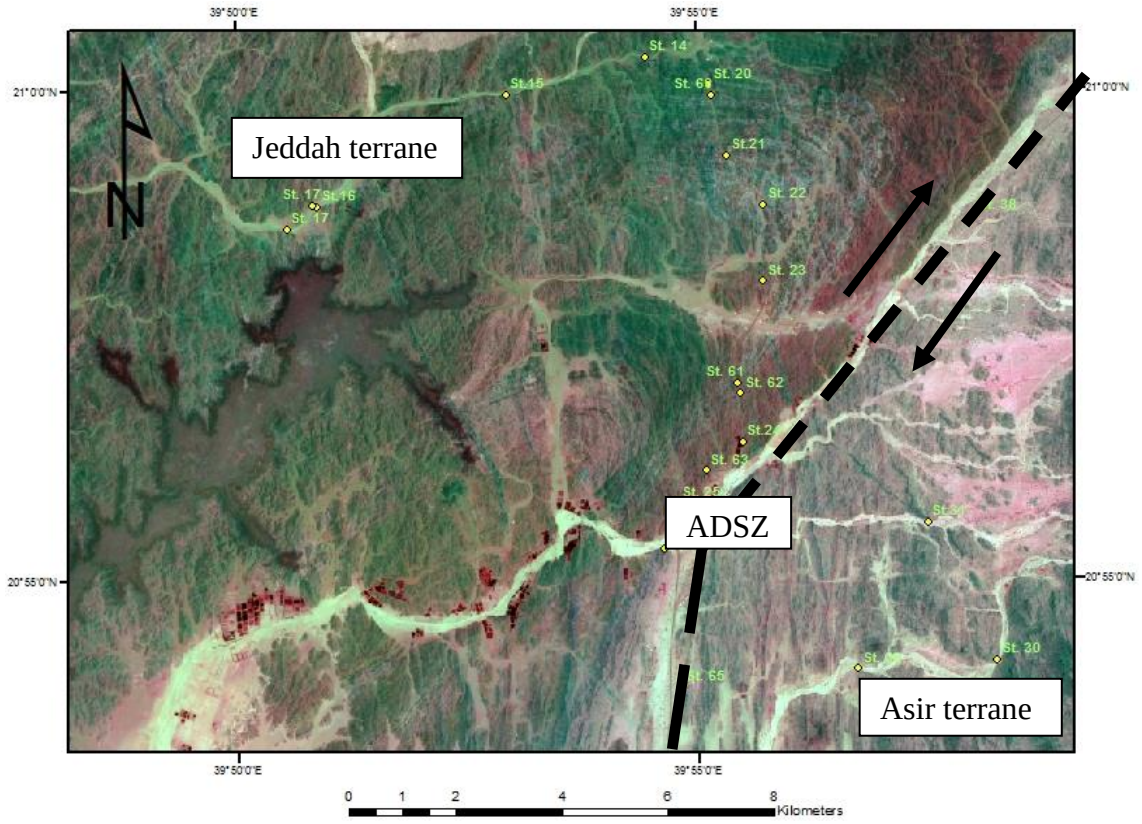

Figure 2.15 SPOT-5 shows the synform drag fold.

2.3 Microstructure Analysis

Microstructural analysis plays a significant role in our research project. It records the internal deformation process when strain accumulates, which leads to change in mineral internal texture, shape and volume. During field work, 21 samples were collected (Figure 2.14) and sent to National Petrographic services, Thin Section Laboratory in Houston. In particular, many thin section samples were carefully selected along ADSZ to interpret the microstructure recorded in mylonitic sheared granites. The lab work was carried out at Carraway building, Florida State University, using a LEICA DMLA microscope.

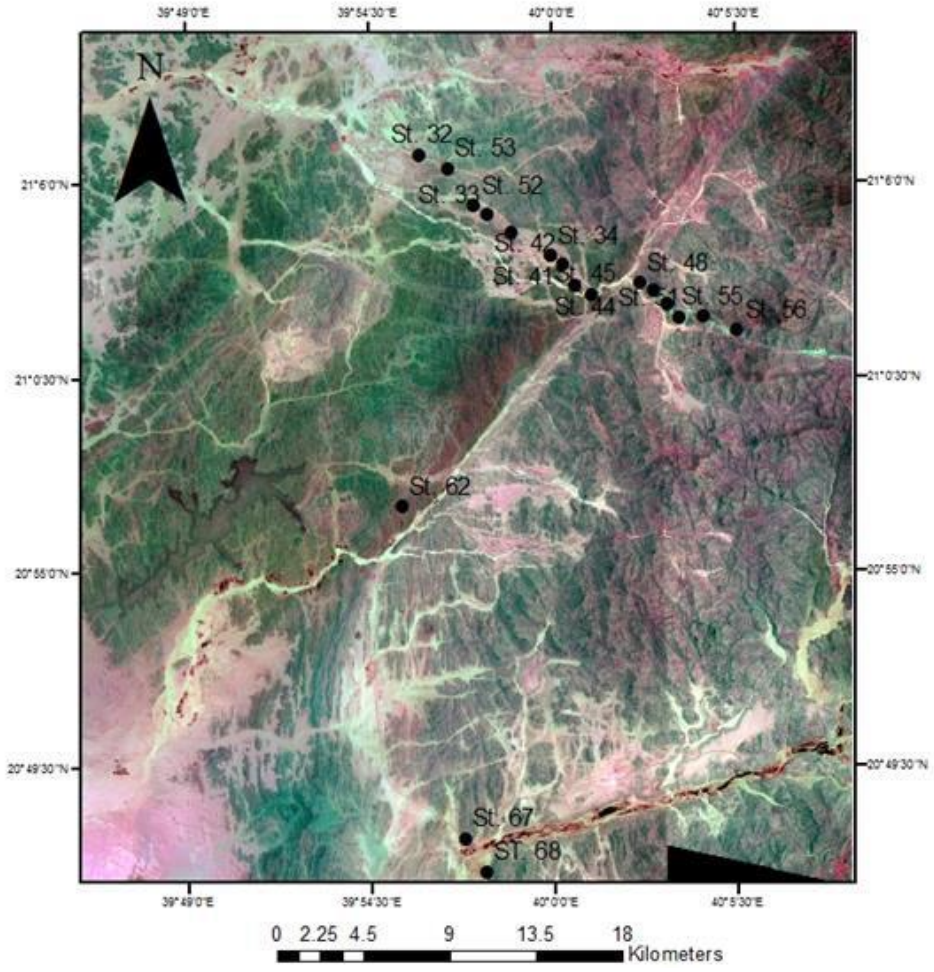

Figure 2.16 Shows the location of selected thin section samples.

Generally, microstructures result from the internal deformation and recrystallization of minerals. They reveal the type of deformation mechanism, deformation process and the kinematic frame work. During high temperature shear deformation, the crystal lattice undergoes not only brittle deformation but also, most importantly, plastic deformation. Microstructure analysis was conducted on 21 thin sections across the study area to demonstrate the type, intensity deformation (Figure 2.14).

The petrographic study shows that the northwestern part of ADSZ (St. 32, 33, 52, 53, and 34) is dominated by heterogeneous granite, amphibolites, and intermediate plutonic rocks (Jeddah terrane) composed mostly of quartz, K- feldspar, microcline, and plagioclase with less than 15% of biotite and hornblende (Figure 2.15). Southeast of the ADSZ (St. 56, 55, and 51) rocks are lithologically characterized as granotoid plutonic bodies (Asir terrane), which contains abundant of quartz, K-feldspar, Plagioclase, and microcline as well as biotite and hornblende also occur (Figure 2.16). ADSZ rocks undergo high degree of recrystallization from igneous textures (St. 42, 44, 45, 48, 49) and are composed of quartz, K-feldspar, plagioclase feldspar, microcline and occasionally biotite and hornblende (more than 25%) (Figure 2.17).

Microstructural study indicates dynamic recrystallization in the mylonitic granites, dominant processes include sub-grain rotation recrystallization and grain boundary migration (St.42B). Grain size reduction and triple junction formation suggest high-temperature recrystallization caused by a volume diffusion mechanism (Figure 2.18). The grain size is an important tool especially for plastic deformation because the smaller grain size, the more strain it has accommodated. In addition, the irregularity in the grain boundaries can be clearly seen in station 42B, and therefore, illustrate dynamic recrystallization and exclude the static recrystallization (Figure 2.18). A few kilometers away from ADSZ, the intensity of the dynamic

recrystallization decreases (St. 50) and samples are governed by recovery, which involves the gradual evolution of sub-grains and deformation bands with undulose extinction (Figure 2.19). Further away from ADSZ, the crystals are very coarse in size and nearly strain free (Figure 2.20). Other microstructures that characterize magmatic features such as deformation twins in plagioclase feldspar (Figure 2.21) and Eutectic minimum composition, which represent a lower melting temperature. (Figure 3.22) can be seen in St. and St. respectively. The deformation twins in the plagioclase feldspar is a result of intracrystalline kink structure that does not involve any fracturing and hence, is classified as plastic deformation mechanism. Intracrystalline fracturing are widespread across thin-section samples (Figure 2.23). Whereas, the intercrystalline fractures are occasionally appeared in some stations (Figure 2.23).

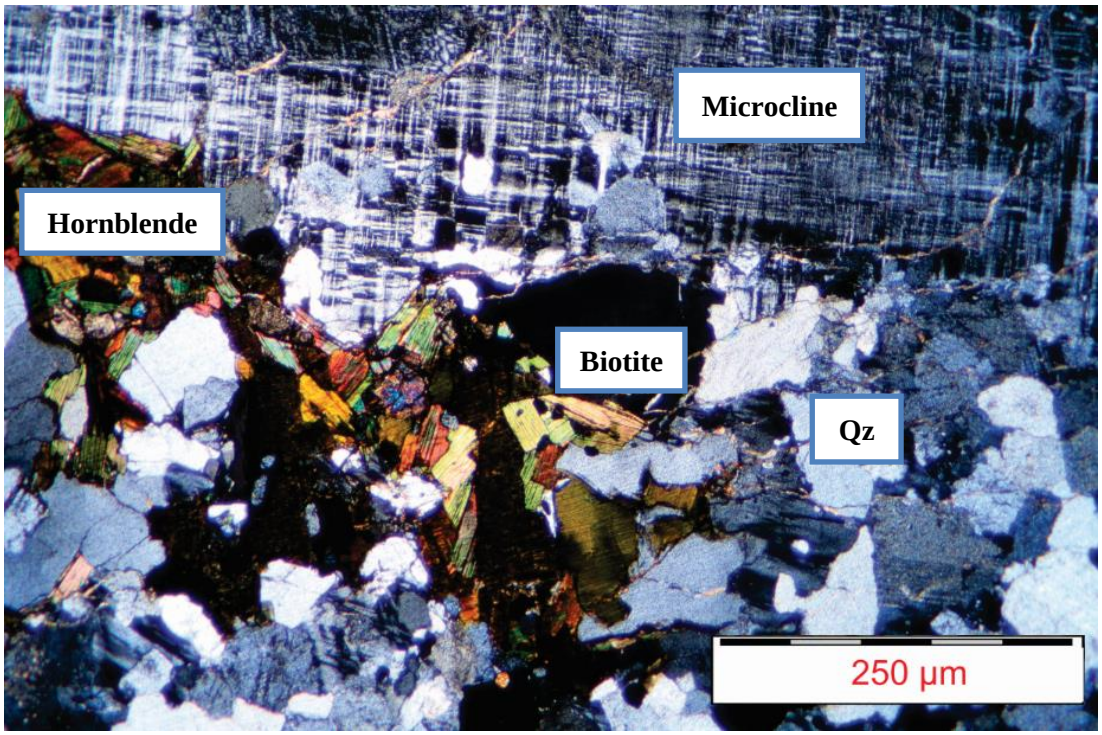

Figure 2.17 Major minerals composition of Jeddah terrane (St. 33).

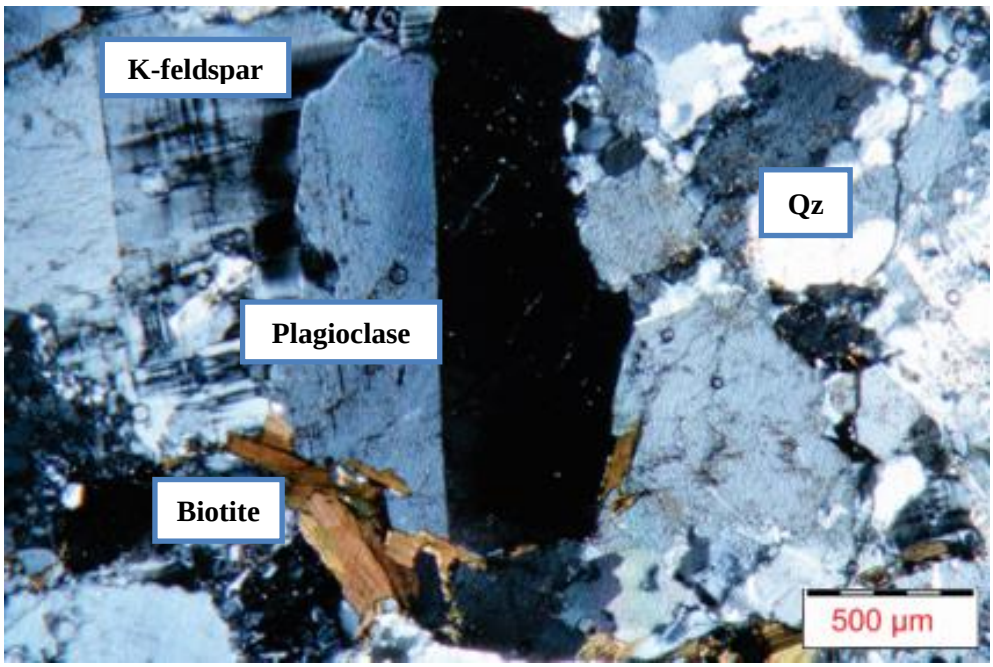

Figure 2.18 Major mineral composition of Asir Terrane (St. 55).

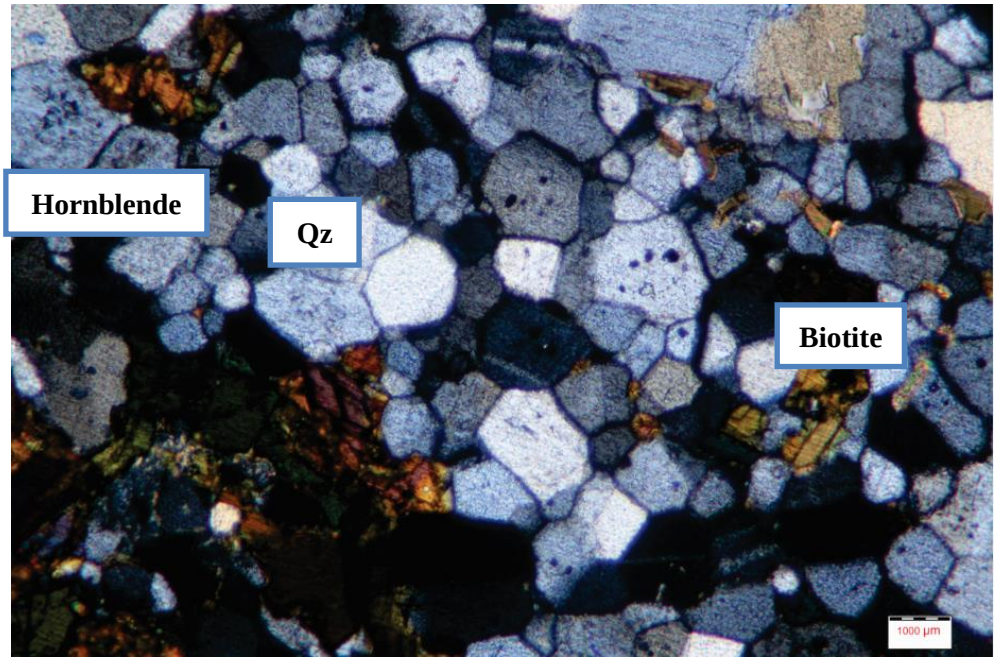

Figure 2.19 High temperature recrystallization and grain size reduction of quartz grains in ADSZ rocks (St. 42).

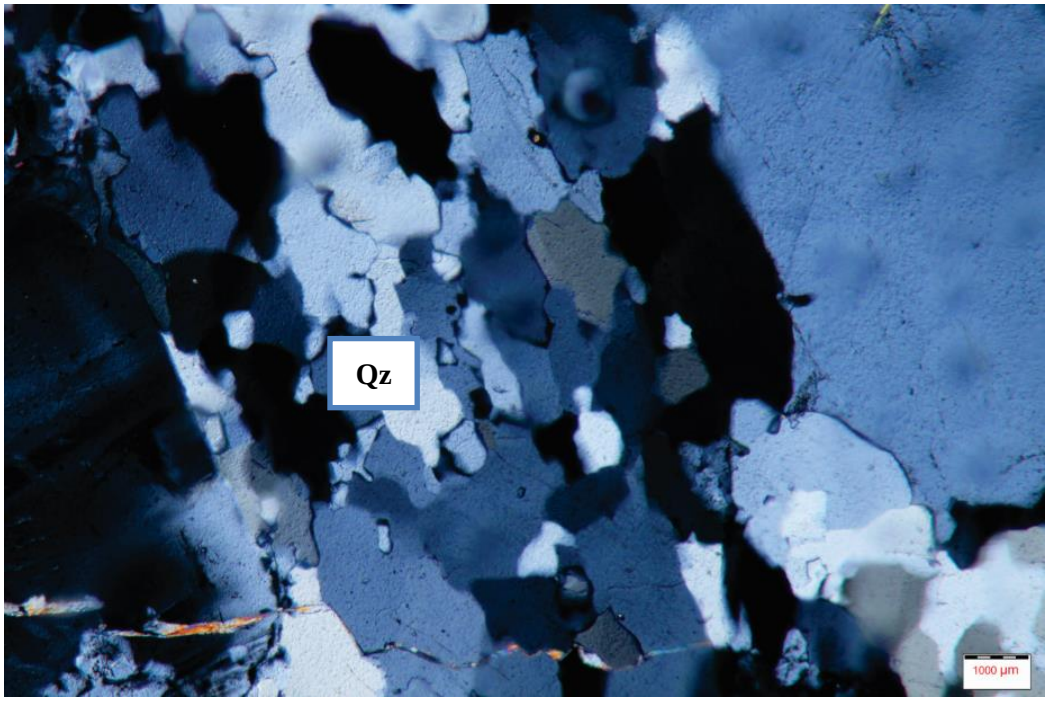

Figure 2.20 The gradual evolution of sub-grains with undulose extinction (St. 50).

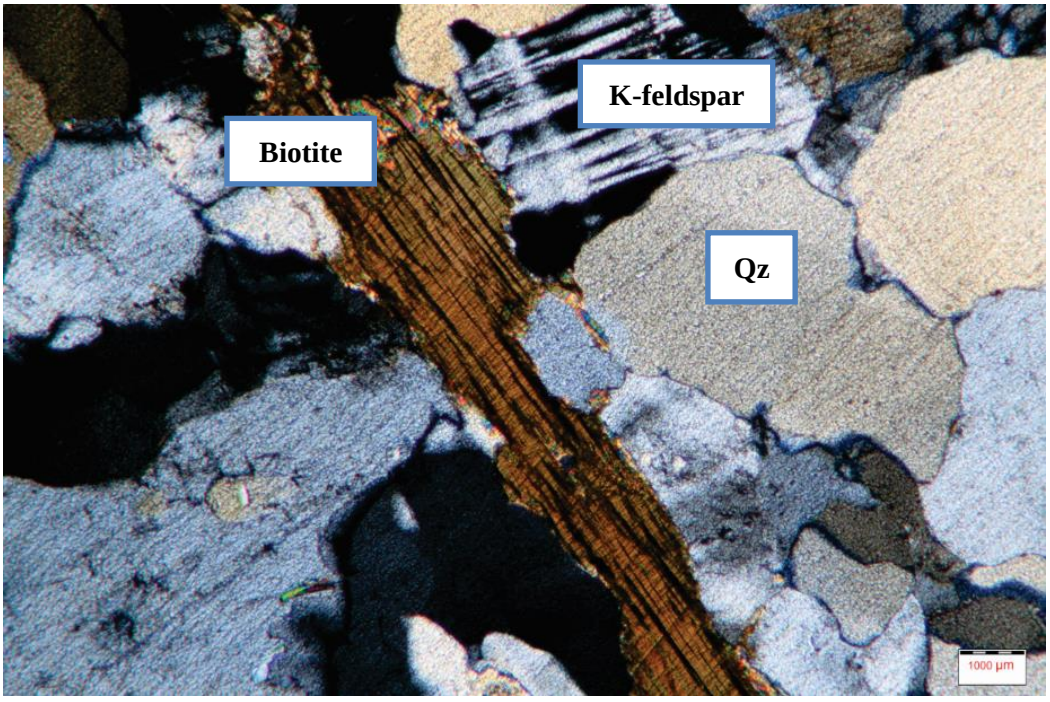

Figure 2.21 Coarse crystalline, magmatic texture (St. 57).

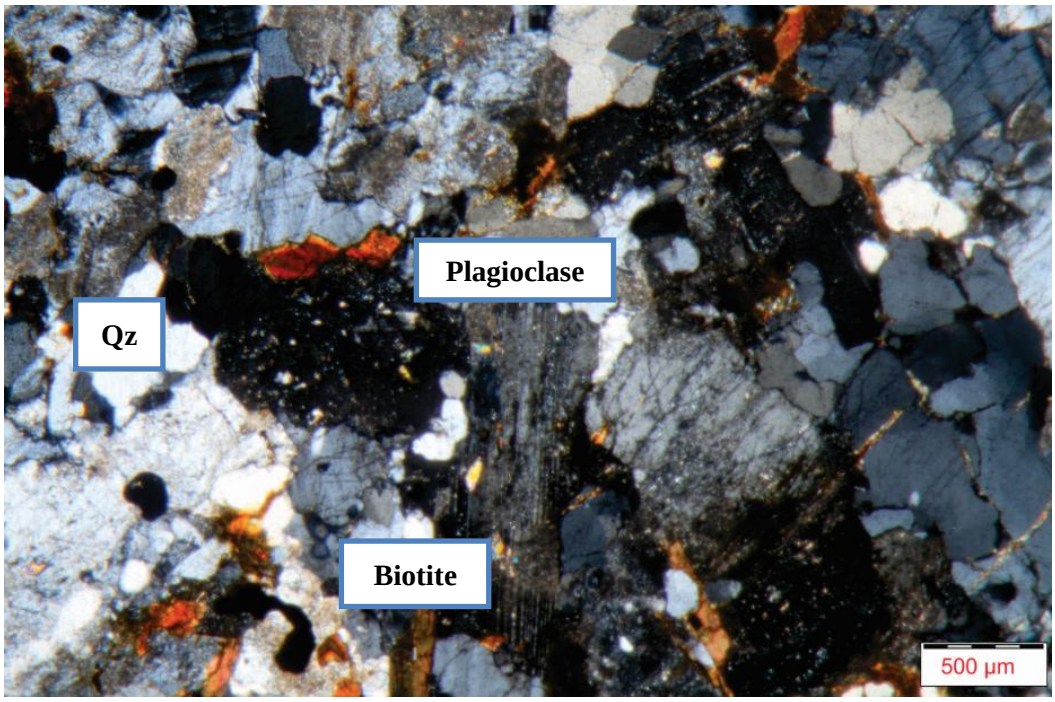

Figure 2.22 Deformation twins in plagioclase feldspar, shows interphingring pattern (St. 68).

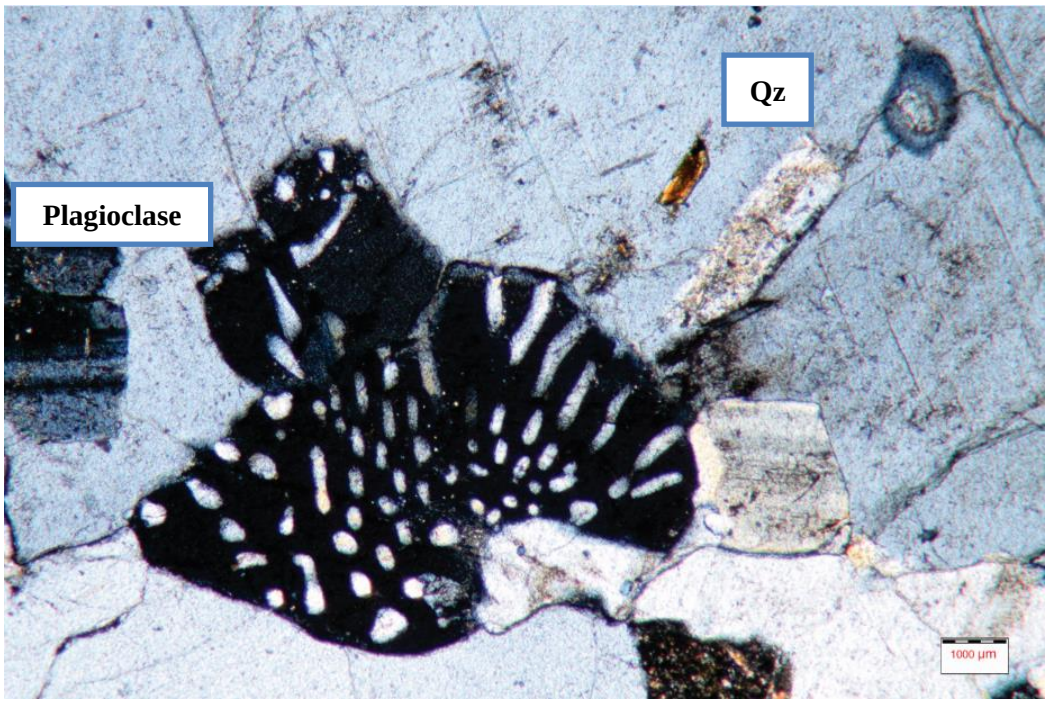

Figure 2.23 Eutectic minimum melt composition, shows lower crystallization temperature (St. 48).

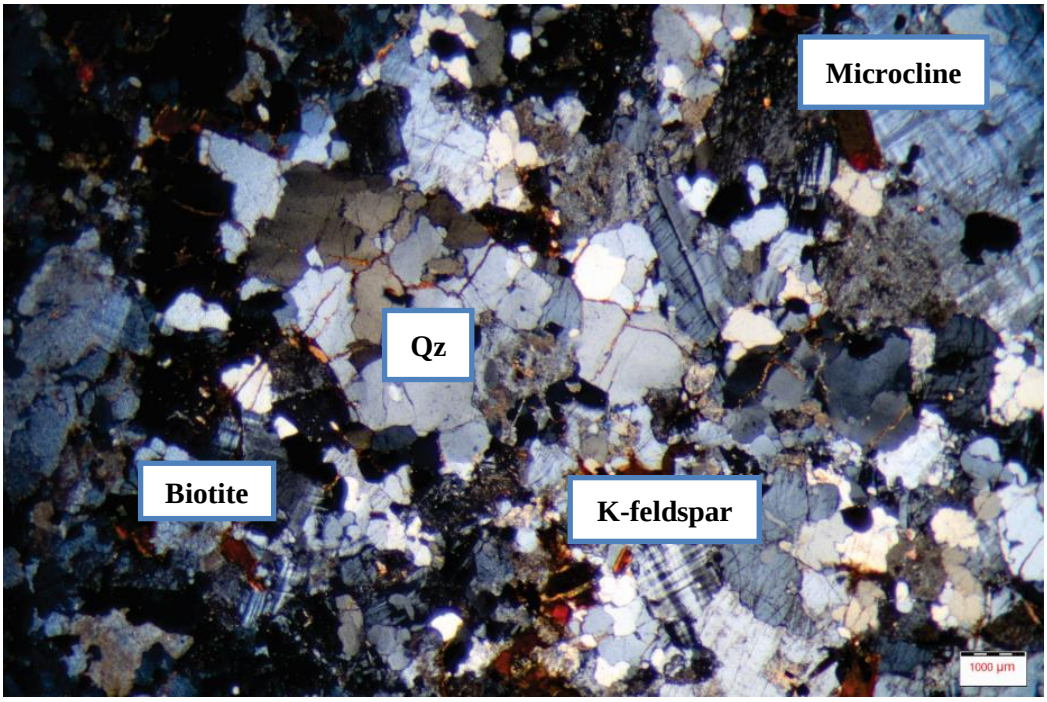

Figure 2.24 Interacrystalline fractures are widespread in thin-section samples (St. 68).

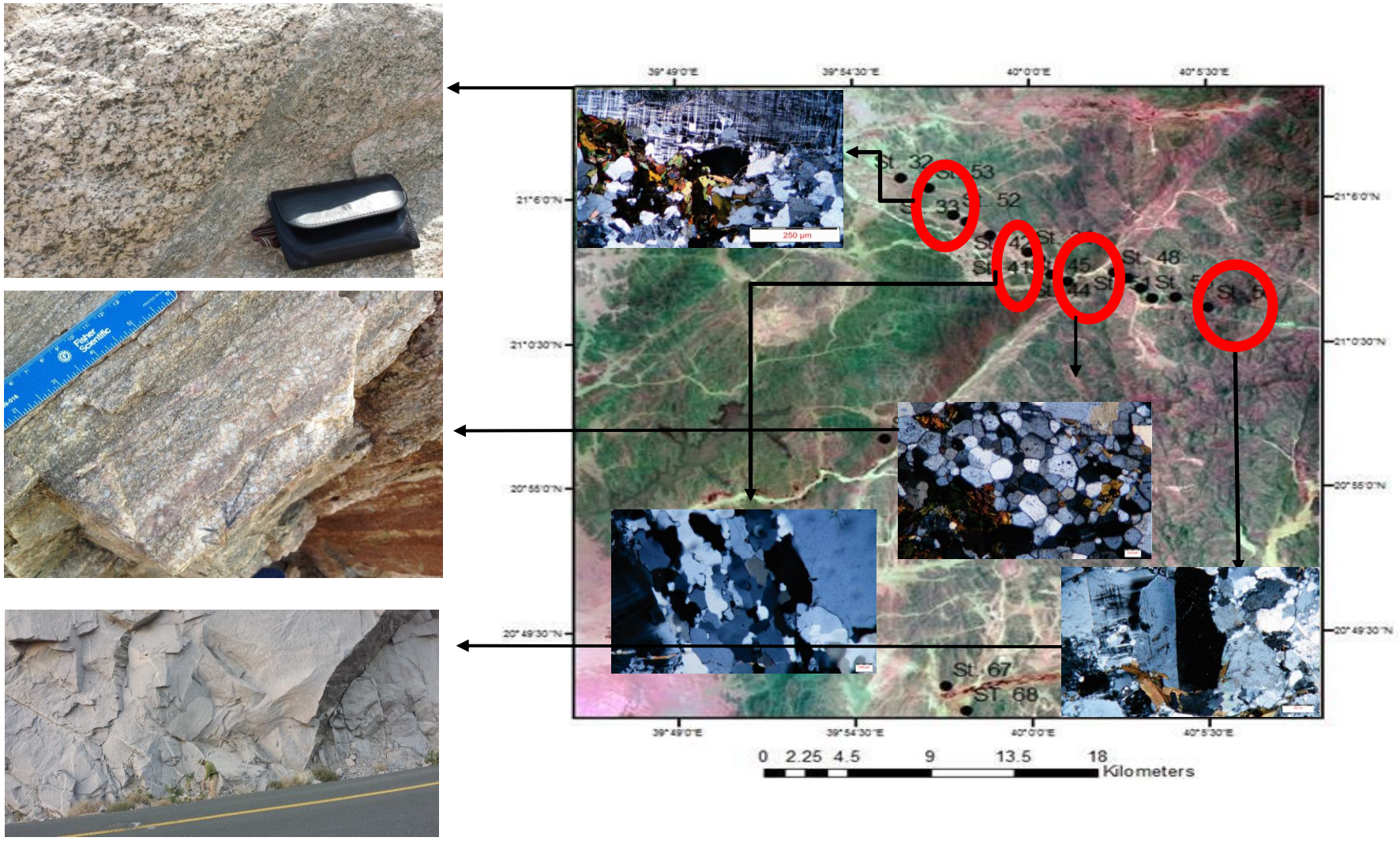

Figure 2.25 displays intensity of recrystallization across ADSZ area.

.

2.4 Whole Rock Geochemistry

Major and trace element Whole rock was conducted using x-ray fluorescence spectrometry (XRF) and inductively coupled plasma – mass spectrometry (ICP-MS). The ICP-MS method was used to determine concentrations of a broad range of trace elements, including rare earth elements (REEs). Whereas XRF; was used to determine major elements compositions. The ICP-MS technique is based on the integration of a high temperature ICP (inductively coupled plasma) source coupled with mass spectrometry. Generally, the analytical material is dissolved using acids and then ionized by ICP source, so that it can be analyzed via the mass spectrometer. Once ions enter the mass spectrometer, they are segregated by their mass/charge ratio.

The theory behind XRF, on the other hand, is that when an electron from the inner orbit is bombarded with x-rays an electron from the outer orbits and the extra energy- formed as result of this transition- is discharged as x- ray photon with specific wave length. The spectra of this florescence allows chemical compositions to be determined.

In this study, the main purpose of using whole rock geochemistry is to determine whether or not the rock samples within the study area are arc, and therefore Proterozoic in age, or rift- related, and therefore Cenozoic. Of particular interest are the various felsic and basaltic dikes, some of which are folded via motion along the ADSZ and some of which cross-cut the shear zone and are clearly post tectonic. During the field work, 26 samples were carefully selected from the Jeddah and Asir terranes, the Ad Damm shear zone, and the Eocene- Miocene Ad Damm dikes complex (Figure 2.14). The samples were sent to ALS geochemistry in Reno, Nevada for lab analysis. The selected analytical packages include:

- ME-ICP06 Whole Rock Package – IC-AES:

Al_2O_3, BaO, CaO, Cr_2O_3, Fe_2O_3, K_2O, MgO, MnO, Na_2O, P_2O_5, SiO_2, SiO_2, SrO, TiO_2.

- ME-MS81 Lithium Borate Fusion – ICP-MS

Ba, Ce, Cr, Cs, Dy, Er, Eu, Ga, Gd, Hf, Ho, La, Lu, Nb, Nd, Pr, Rb, Sm, Sn, Sr, Ta, Tb, Th, Tm, U, V, W, Y, Yb, Zr.

- ME-4ACD81 Base Metals by 4-acid dig

Ag, As, Cd, Co, Cu, Li, Mo, Ni, Pb, Sc, TI, Zn.

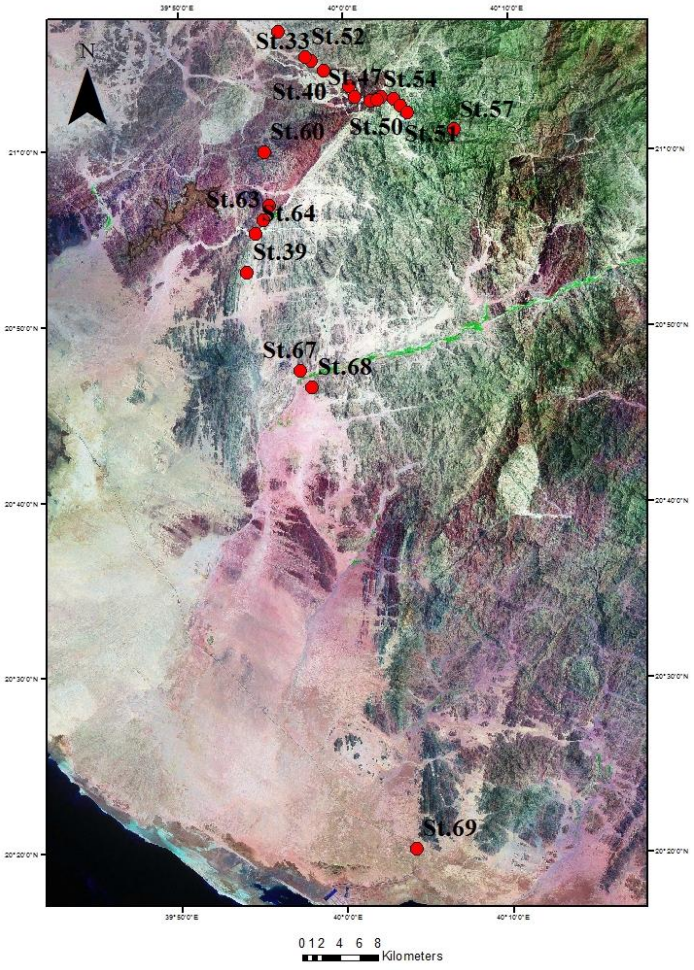

Figure 2.26 Mr-SID displays samples location.

2.4.1 Major Elements

One of the applications of major elements geochemistry (Si, Ti, Al, Fe, Mn, Mg, Ca, K, Na, P,) is to give a proper classification of rocks using oxide-oxide plots or cation classification (Rollinson, 1993). Many diagrams have been used here to understand the relationship between the different elements within individual rocks, and therefore, obtain a comprehensive knowledge about the geochemical processes of the magmatic rocks.

First, the oxide-oxide plot displays a fundamental role in classifying igneous rocks. The total alkalis-silica diagram (TAS) is made by plotting SiO_2 on x-axis against the sum of potassium and sodium oxides on the y-axis (Figure 2.25) (Le Maitre et al., 1989). TAS chart indicates that the granitoid bodies of the Jeddah terrane, Asir terrane, and ADSZ rocks have similar and high concentration of SiO2, K2O, and Na2O. However, the Jeddah terrane contains extensive mafic (mainly mata-basalt and amphibolite) and intermediate plutonic compositions, whereas the Asir does not. Eocene-Miocene Ad Damm dikes complex are mainly basaltic in composition with SiO_2 concentrations between 50-45 wt. percent.

Secondly, the K_2O vs SiO_2 classification diagram of Le Maitre et al. (1989), was used to distinguish between low, medium, and high potassium series rocks (Figure 2.26). The chart illustrates that most of granitic rock units of Asir, Jeddah, ADSZ, and Folded silicic dikes of Ad Damm drag fold are characterized as high- K calc- alkaline in composition. Several samples of the Jeddah terrane are characterized as medium- K- calc alkaline, which reflects the heterogeneous composition of Jeddah terrane. The mafic group, which includes meta-basalt, amphibolite (Jeddah terrane host rock), Eocene-Miocene Ad Damm dikes complex basalt, folded basaltic dikes, plot in the low to medium k- calc alkaline fields.

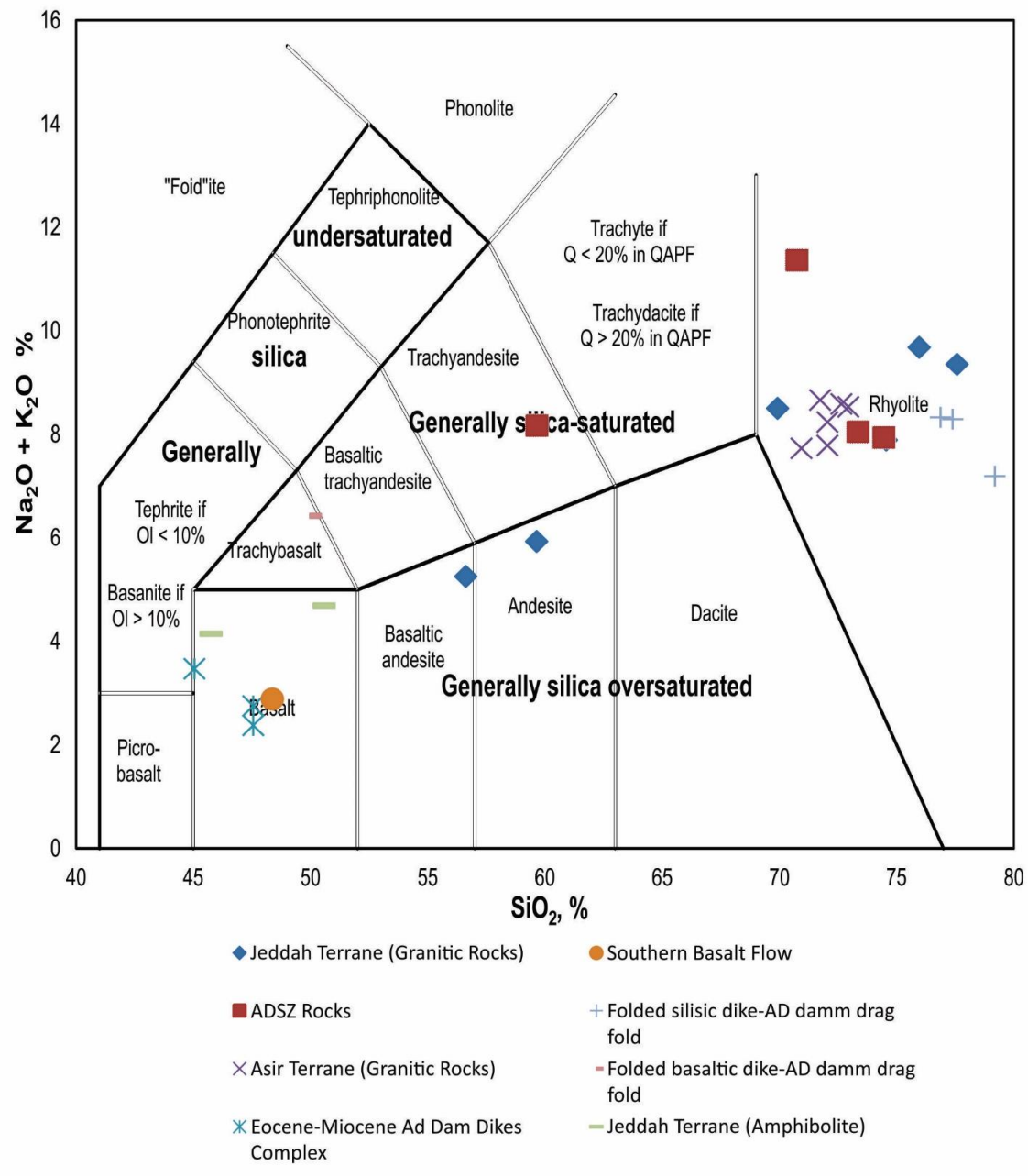

Figure 2.27 Classification of volcanic and plutonic rocks by using the concentration of the total Alkalis vs. SiO_2.

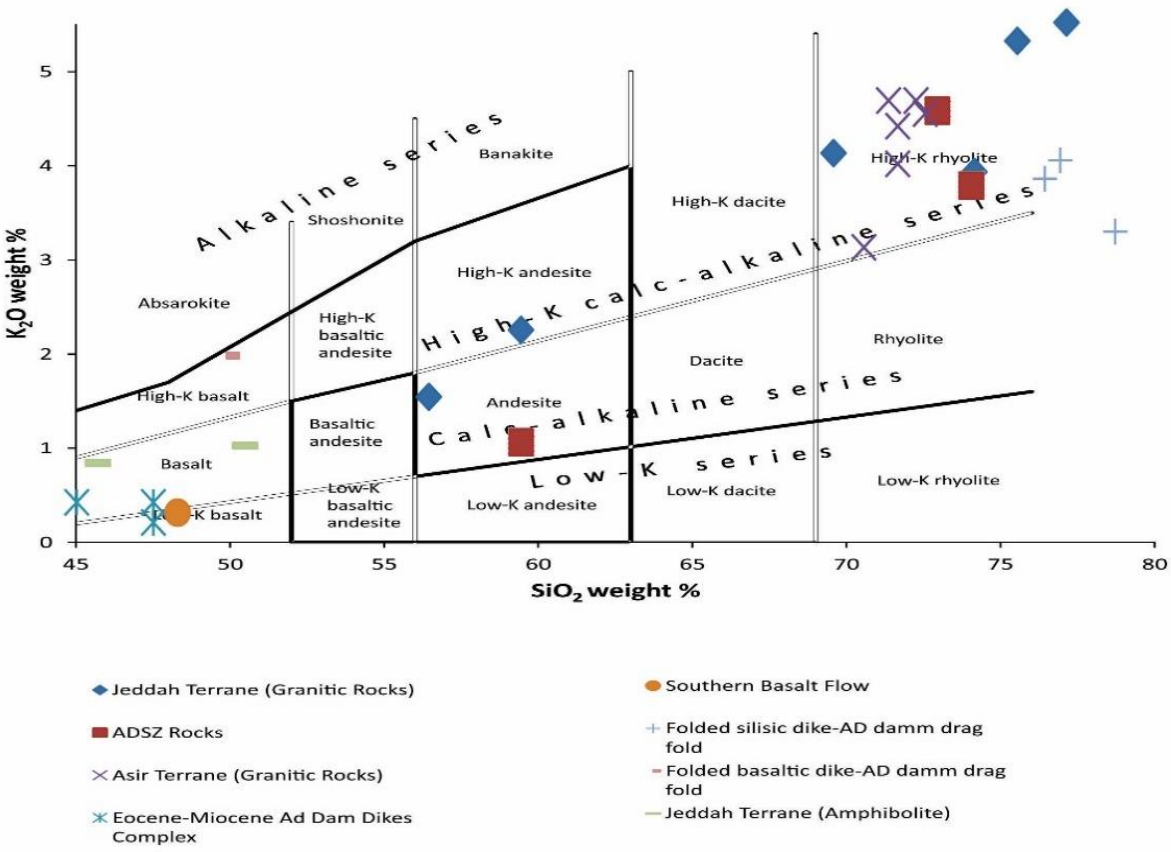

Figure 2.28 Sub-alkaline classification using the concentration of SiO_2 and K_2O (Le Maitre et al., 1989).

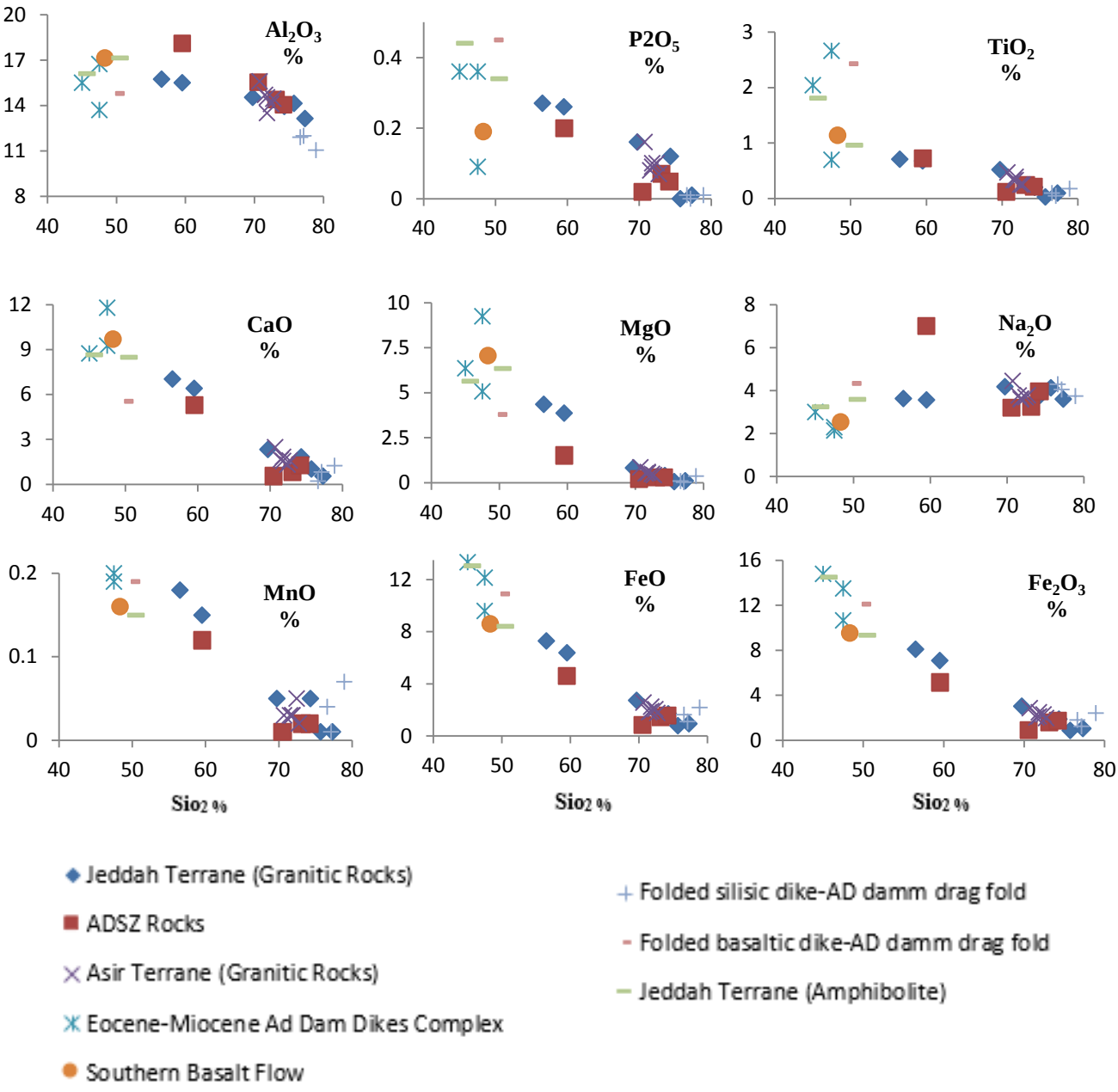

Figure 2.29 Harker variation diagram of major elements from Jeddah, Asir terranes and ADSZ rocks, western Saudi Arabian margin.

Thirdly, Harker variation diagrams (Figure 3.18) shows a strong correlation between most of the major elements of the different geologic units verses SiO_2. CaO, MgO, MnO, FeO, Fe_2O_3, TiO_2, and P_2O_5 decrease with increase SiO_2. Whilst, K_2O and the sum of $K_2O$and Na_2O increase dramatically with increasing of SiO_2. The percentage of AL_2O_3 remains almost constant with slightly increase during the formation of the basaltic dikes. This indicates that most of plutonic rock units are high- silica rich value (SiO2= 70-80%). While the basaltic dikes from different ages have silica value ranging from 45-55%.

Finally, the cation classification or R1-R2 diagram was constructed to display the cations distribution of the sample (De la Roche et al., 1980). The oxide compounds are divided by their molecular weights and then multiplied by their number of cations (Table 3.1). This diagram is very suitable for classifying the plutonic rocks (Figure 3.19), because it utilizes most of the major elements (Rollinson, 1993). R1-R2 parameters are plotted on x-y axis respectively, by calculating R_1= 4Si – 11(Na + K) – 2(Fe + Ti) and R_2= 6Ca + 2Mg + Al (De la Roche et al., 1980). The chart shows samples taken from Ad Damm folded silicic dikes are classified as alkali granite, while the granitoid bodies Asir and Jeddah terranes are characterized as granite. Two samples of Jeddah terranes (St. 44 and 42) are classified as monzo-diorite, which supports Jeddah terrane has heterogeneous composition. Volcanic rocks are also classified using this diagram, and the Eocene-Miocene Ad Damm dike complex rocks are categorized as monzo gabbro to gabbro diorite, while the meta-basalt and amphibolite are defined as syeno-basalt to monzo-basalt in composition. However the folded basaltic dikes are classified as syeno- andesite. On the other hand, the classification ADSZ rocks using R1-R2 parameters is not very clear because most of its rock units under went significant dynamic recrystallization, which in turn, may have altered the chemical composition.

Table 2.2 Cation calculation for R1-R2 diagram.

SAMPLE	SiO2	Al2O3	FeO	Fe2O3	CaO	MgO	Na2O	K2O	TiO2	MnO	P2O5	Cation pro.SiO2	Cation pro.Al2O3	Cation pro.FeO	Cation pro.Fe2O3	Cation pro.CaO	Cation pro.MgO	Cation pro.Na2O	Cation pro.K2O	Cation pro.TiO2	Cation pro.MnO
DESCRIPTION	%	%	%	%	%	%	%	%	%	%	%	ppb	ppb	ppb	ppb	ppb	ppb	ppb	ppb	ppb	ppb
St. 32A	69.7	14.55	2.717396	3.02	2.32	0.82	4.18	4.21	0.52	0.05	0.16	1.144499179	0.285406042	0.037820404	0.037823283	0.041369472	0.020347395	0.13488222	0.089384289	0.006508135	0.000704821
St. 33A	75.7	14.15	0.773828	0.86	1.02	0.05	4.13	5.43	0.03	0.01	0.009	1.243021346	0.277559827	0.010770049	0.010770869	0.018188302	0.001240695	0.133268796	0.115286624	0.000375469	0.000140964
St. 40	77.3	13.15	0.926794	1.03	0.54	0.1	3.6	5.63	0.1	0.01	0.01	1.269293924	0.257944292	0.012899012	0.012899994	0.009629101	0.00248139	0.116166505	0.119532909	0.001251564	0.000140964
St. 42B	56.5	15.75	7.279382	8.09	7.03	4.35	3.62	1.55	0.71	0.18	0.27	0.927750411	0.308944684	0.101313598	0.10132131	0.125356633	0.107940447	0.116811875	0.032908705	0.008886108	0.002537356
St. 44 (1)	59.5	15.5	6.370584	7.08	6.41	3.86	3.56	2.28	0.68	0.15	0.26	0.977011494	0.3040408	0.088665052	0.088671802	0.114300999	0.095781638	0.114875766	0.048407643	0.008510638	0.002114463
St. 52	74.3	13.95	1.691624	1.88	1.83	0.39	3.78	4	0.2	0.05	0.12	1.220032841	0.27363672	0.023543827	0.02354562	0.032631954	0.009677419	0.121974831	0.08492569	0.002503129	0.000704821
St. 60C	50.5	17.15	8.395134	9.33	8.49	6.34	3.59	1.02	0.96	0.15	0.34	0.829228243	0.336406434	0.116842505	0.1168514	0.15139087	0.157320099	0.115843821	0.021656051	0.012015019	0.002114463
St. 62B	45.7	16.1	13.0471	14.5	8.64	5.63	3.24	0.83	1.81	0.23	0.44	0.750410509	0.315810122	0.181588031	0.181601854	0.154065621	0.139702233	0.104549855	0.017622081	0.022653317	0.003242176
St. 46	59.5	18.1	4.63397	5.15	5.33	1.52	7.01	1.05	0.73	0.12	0.2	0.977011494	0.355041193	0.064495059	0.064499969	0.095042796	0.037717122	0.226202001	0.022292994	0.009136421	0.00169157
St. 47	70.5	15.55	0.827816	0.92	0.57	0.21	3.22	8.01	0.13	0.01	0.02	1.157635468	0.305021577	0.011521447	0.011522325	0.010164051	0.005210918	0.103904485	0.170063694	0.001627034	0.000140964
St. 49	73.1	14.4	1.43968	1.6	0.82	0.32	3.27	4.67	0.24	0.02	0.07	1.200328407	0.282463711	0.0200373	0.020038825	0.014621969	0.007940447	0.105517909	0.099150743	0.003003755	0.000281928
St. 54	74.2	14.05	1.583648	1.76	1.26	0.32	3.98	3.85	0.21	0.02	0.05	1.218390805	0.275598274	0.02204103	0.022042708	0.022467903	0.007940447	0.128428525	0.081740977	0.002628285	0.000281928
St. 50	71.5	14.7	1.817596	2.02	1.64	0.51	3.77	4.78	0.33	0.03	0.08	1.174055829	0.288348372	0.025297091	0.025299017	0.029243937	0.012655087	0.121652146	0.1014862	0.004130163	0.000422893
St. 51	71.8	13.5	2.231504	2.48	1.56	0.59	3.59	4.09	0.39	0.03	0.1	1.178981938	0.264809729	0.031057815	0.031060179	0.027817404	0.014640199	0.115843821	0.086836518	0.004881101	0.000422893
St. 57	71.8	14.55	1.907576	2.12	1.83	0.54	3.63	4.5	0.33	0.03	0.09	1.178981938	0.285406042	0.026549422	0.026551443	0.032631954	0.013399504	0.11713456	0.095541401	0.004130163	0.000422893
St. 65	70.7	15.6	2.56443	2.85	2.47	0.85	4.44	3.18	0.47	0.03	0.16	1.16091954	0.306002354	0.035691441	0.035694157	0.044044223	0.021091811	0.143272023	0.067515924	0.005882353	0.000422893
St. 67	72.7	14.45	1.763608	1.96	1.6	0.42	3.78	4.64	0.25	0.02	0.07	1.193760263	0.283444488	0.024545692	0.024547561	0.02853067	0.010421836	0.121974831	0.0985138	0.003128911	0.000281928
St. 68	72.4	14.1	2.051544	2.28	1.31	0.48	3.69	4.78	0.25	0.05	0.1	1.188834154	0.276579051	0.028553152	0.028555326	0.023359486	0.01191067	0.119070668	0.1014862	0.003128911	0.000704821
St. 60A	76.6	11.9	1.61964	1.8	0.22	0.09	4.29	3.93	0.1	0.04	0.01	1.257799672	0.233424872	0.022541962	0.022543678	0.003922967	0.002233251	0.138431752	0.08343949	0.001251564	0.000563857
St. 62A	77.1	12	1.106754	1.23	0.82	0.03	4.05	4.13	0.05	0.01	0.009	1.266009852	0.235386426	0.015403674	0.015404847	0.014621969	0.000744417	0.130687318	0.087685775	0.000625782	0.000140964
St. 64A	78.9	11.05	2.177516	2.42	1.24	0.37	3.74	3.35	0.18	0.07	0.01	1.295566502	0.216751667	0.030306416	0.030308723	0.02211127	0.009181141	0.120684092	0.071125265	0.002252816	0.000986749
St. 63C	49.9	14.8	10.88758	12.1	5.54	3.78	4.33	2	2.43	0.19	0.45	0.819376026	0.290309925	0.151532081	0.151543616	0.098787447	0.093796526	0.139722491	0.042462845	0.030413016	0.00267832
St. 39	47.5	16.75	9.58287	10.65	11.8	9.24	2.14	0.18	0.7	0.19	0.09	0.779967159	0.32856022	0.133373278	0.13338343	0.210413695	0.229280397	0.069054534	0.003821656	0.008760951	0.00267832
St. 33C	47.5	13.7	12.1473	13.5	9.26	5.07	2.29	0.4	2.66	0.2	0.36	0.779967159	0.268732836	0.169064718	0.169077588	0.165121255	0.125806452	0.073894805	0.008492569	0.033291615	0.002819284
St. 64C	45	15.5	13.31704	14.8	8.74	6.35	3	0.4	2.04	0.23	0.36	0.738916256	0.3040408	0.185345024	0.185359133	0.155848787	0.157568238	0.096805421	0.008492569	0.025531915	0.003242176
St. 69	48.3	17.15	8.584092	9.54	9.7	7.06	2.53	0.29	1.14	0.16	0.19	0.793103448	0.336406434	0.119472401	0.119481495	0.17296719	0.175186104	0.081639238	0.006157113	0.014267835	0.002255427

Table 2.2 (Continued).

SAMPLE	Cation.SiO2	Cation.Al2O3	Cation.FeO	Cation.Fe2O3	Cation.CaO	Cation.MgO	Cation.Na2O	Cation.K2O	Cation.TiO2	Cation.MnO	Cation.P2O5	R1	R2
DESCRIPTION	Milli	Milli	Milli	Milli	Milli	Milli	Milli	Milli	Milli	Milli	Milli		
St. 32A	1144.499179	285.4060416	2717.396	37.82328261	41.36947218	20.34739454	134.8822201	89.38428875	6.508135169	0.704820975	2.2543149	2022.402283	574.3176638
St. 33A	1243.021346	277.5598274	773.828	10.77086856	18.18830243	1.240694789	133.2687964	115.2866242	0.375469337	0.140964195	0.126805213	2215.683084	389.1710315
St. 40	1269.293924	257.9442919	926.794	12.89999374	9.629101284	2.481389578	116.1665053	119.5329087	1.251564456	0.140964195	0.140894681	2456.179027	320.6816787
St. 42B	927.7504105	308.9446842	7279.382	101.32131	125.3566334	107.9404467	116.8118748	32.90870488	8.886107635	2.537355512	3.804156393	1843.66043	1276.965378
St. 44 (1)	977.0114943	304.0408003	6370.584	88.67180162	114.3009986	95.78163772	114.8757664	48.40764331	8.510638298	2.114462926	3.663261712	1917.563591	1181.410067
St. 52	1220.032841	273.6367203	1691.624	23.54561964	32.63195435	9.677419355	121.9748306	84.92569002	2.503128911	0.704820975	1.690736175	2552.128139	488.7832851
St. 60C	829.228243	336.4064339	8395.134	116.8513996	151.3908702	157.3200993	115.8438206	21.65605096	12.01501877	2.114462926	4.790419162	1546.681548	1559.391854
St. 62B	750.410509	315.8101216	13047.1	181.6018536	154.0656205	139.7022333	104.5498548	17.62208068	22.65331665	3.242176487	6.199365974	1249.240405	1519.608311
St. 46	977.0114943	355.0411926	4633.97	64.49996869	95.04279601	37.71712159	226.2020006	22.29299363	9.136420526	1.691570341	2.817893625	1027.328262	1000.732212
St. 47	1157.635468	305.0215771	827.816	11.5223245	10.16405136	5.210918114	103.9044853	170.0636943	1.627033792	0.140964195	0.281789362	1590.59318	376.4277214
St. 49	1200.328407	282.4637113	1439.68	20.03882522	14.62196862	7.94044665	105.517909	99.1507431	3.003754693	0.28192839	0.986262769	2503.873296	386.0764163
St. 54	1218.390805	275.5982738	1583.648	22.04270775	22.467903	7.94044665	128.4285253	81.74097665	2.628285357	0.28192839	0.704473406	2512.35671	426.2865851
St. 50	1174.055829	288.3483719	1817.596	25.29901685	29.24393723	12.65508685	121.6521459	101.4861996	4.130162703	0.422892585	1.12715745	2182.843158	489.122169
St. 51	1178.981938	264.8097293	2231.504	31.0601791	27.81740371	14.64019851	115.8438206	86.83651805	4.881101377	0.422892585	1.408946812	2414.561464	460.9945486
St. 57	1178.981938	285.4060416	1907.576	26.55144342	32.63195435	13.39950372	117.1345595	95.54140127	4.130162703	0.422892585	1.268052131	2315.128969	507.9967751
St. 65	1160.91954	306.0023539	2564.43	35.69415743	44.04422254	21.09181141	143.2720232	67.51592357	5.882352941	0.422892585	2.2543149	2241.857725	612.4513119
St. 67	1193.760263	283.444488	1763.608	24.5475609	28.53067047	10.42183623	121.9748306	98.51380042	3.128911139	0.28192839	0.986262769	2294.313166	475.4721833
St. 68	1188.834154	276.5790506	2051.544	28.55532594	23.35948645	11.91066998	119.070668	101.4861996	3.128911139	0.704820975	1.408946812	2265.8426	440.5573092
St. 60A	1257.799672	233.4248725	1619.64	22.54367838	3.92296719	2.23325062	138.4317522	83.43949045	1.251564456	0.56385678	0.140894681	2543.024532	261.4291769
St. 62A	1266.009852	235.386426	1106.754	15.40484689	14.62196862	0.744416873	130.6873185	87.68577495	0.625782228	0.140964195	0.126805213	2629.874123	324.6070715
St. 64A	1295.566502	216.7516673	2177.516	30.30872315	22.11126961	9.181141439	120.6840916	71.12526539	2.25281602	0.986749366	0.140894681	3007.240004	367.7815679
St. 63C	819.3760263	290.3099255	10887.58	151.5436158	98.7874465	93.79652605	139.7224911	42.46284501	30.41301627	2.678319707	6.340260655	909.5521435	1070.627657
St. 39	779.9671593	328.5602197	9582.87	133.3834304	210.4136947	229.280397	69.05453372	3.821656051	8.760951189	2.678319707	1.268052131	2033.941786	2049.603182
St. 33C	779.9671593	268.7328364	12147.3	169.0775878	165.1212553	125.8064516	73.89480478	8.492569002	33.29161452	2.819283902	5.072208524	1808.869121	1511.073272
St. 64C	738.9162562	304.0408003	13317.04	185.3591333	155.8487874	157.5682382	96.8054211	8.492569002	25.53191489	3.242176487	5.072208524	1375.605037	1554.270001
St. 69	793.1034483	336.4064339	8584.092	119.4814954	172.9671897	175.1861042	81.63923846	6.157112527	14.26783479	2.255427122	2.676998943	1939.155272	1724.581781

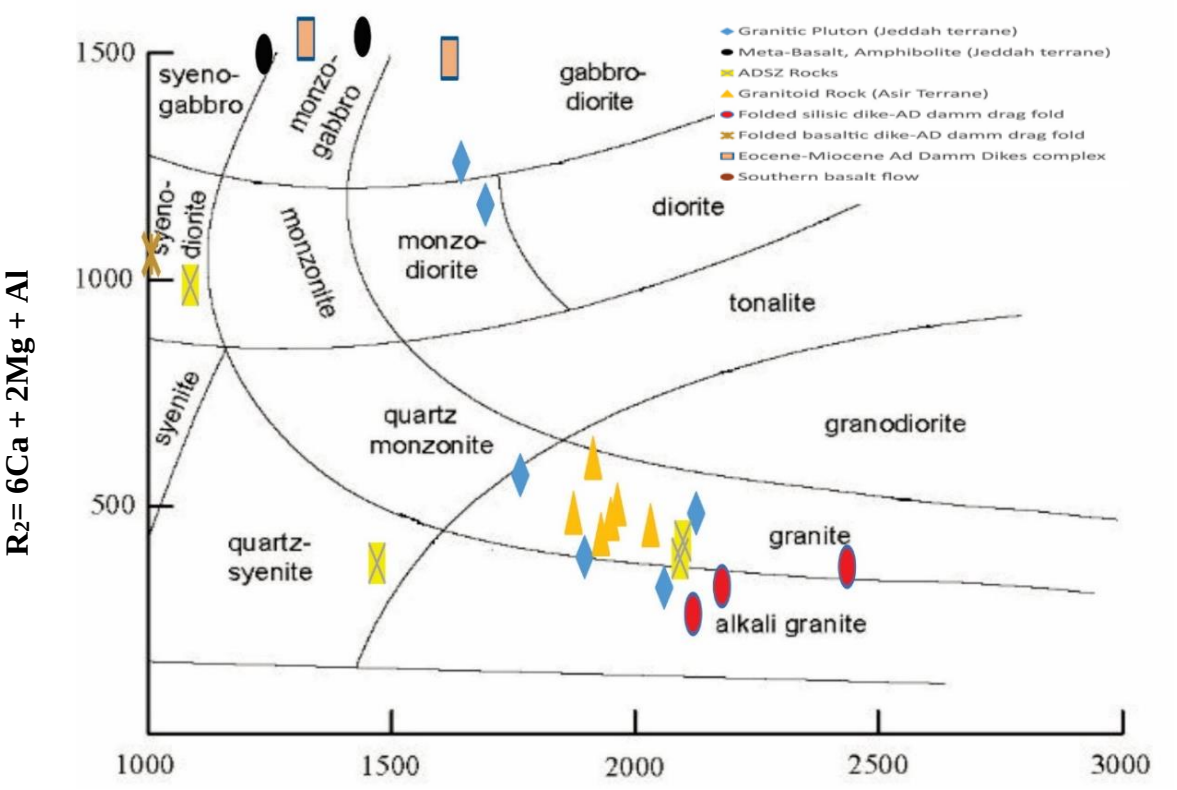

R_1= 4Si – 11(Na + K) – 2(Fe +Te)

Figure 2.30 Classification of plutonic rocks using R1-R2.

2.4.2 Trace Elements Geochemistry

The different samples, collected during the field work, were grouping on the basis of their geochronological dates, lithological difference, and field relation into 6 main groups as follow: Jeddah terrane, Asir terrane, ADSZ rocks, Eocene-Miocene basaltic dikes, folded Silicic dikes (in the Ad Damm drag folds), and folded basaltic host rock of Ad Damm drag folds (Figure 3.20). The spider element diagrams show that all six groups are defined by high concentration of large ion lithophies (LILE's) (Cs, Rb, K, Ba, Sr) compared to the high field strength elements HFSE (Th, U, Ce, Ti, Nb, Ta, Zr, Hf) and oheavy rare earth elements (HREE). However, the Neoproterozoic rocks are characterized by a large negative Nb-Ta anomaly, suggesting an arc origin consistent with that of previous worker (Rollinson, 1993). In contrast, the Cenozoic groups (Ad Damm dike complex and the southern basaltic flow) exhibit a significantly reduced negative Nb-Ta anomaly that is consistent with a rift origin.

In detail, the spider diagram displays that both the Jeddah terrane (which includes granitic plutons, silicic & basaltic folded dikes, and amphibolite/ meta-basalt), Asir terrane, and ADSZ rocks have broadly similar trace element patterns, which suggests that they may originated in similar tectonic environments (Figure 3.21). Normalized multi-element diagrams exhibit that large ion lithophile elements (LILE) are elevated in composition. Whereas high field strength elements (HFSE) are depleted. The plutonic and volcanic groups listed above are characterized by an arc-related signature, which reflect the magmatic origin of the Jeddah and Asir terranes during Neoproterozoic (Hamimi et al., 2014). The rare earth element pattern are defined by sharp slop where the average of light rare earth elements to heavy rare earth elements $(Ce/Yb)_n$ ranging between 2- 28 and the average of LILE to HFSE ranges between (K/Ta) 15-8. The highest LREE/HREE content and LILE/HFSE belongs to Asir terrane where $(Ce/Yb)_n$= 28 and (K/Ta)=

22-8. While the lowest fractionation ratios and LILE/HFSE dominate the folded basaltic and silicic dikes as well as amphibolite of Jeddah terrane (Table 2.3).

In contrast, Eocene-Miocene basaltic dikes and southern basaltic flow are distinguished from the other groups by a significantly reduced Nb-Ta anomaly, which is consistent with a rift-related environment of formation (Figure 3.21). The rare earth element pattern is defined by the slop between LREE/HREE $(Ce/Yb)_n$ ranging between 2.1- 2.3 and the average of LILE to HFSE fluctuated (K/Ta) between 1.1- 2.2. LIL elements have slightly enrichment content (Cs, Rb, Ba, K, Sr) relative to the older groups. Whereas, HFS elements have relatively less depletion in their content (Nb, Ta, U, Zr, Hf, Ti).

Table 2.3 Normalized trace element values to (to N-MORB (Klein, 2003)), average calculation of LREE/HREE (Ce/Yb), and ratio of LILE to HFSE (Ba/Nb).

Normalized values to N-MORB (Klein, 2003)																							
REE	Cs	Rb	Ba	Th	U	Nb	Ta	K	La	Ce	Sr	Nd	Zr	Hf	Sm	Eu	Ti	Tb	Dy	Yb	Lu	Ce/Yb	Ba/Nb
Rock Unit																							
Granitic Pluton (Jeddah terrane)	13.95062	42.70115	63.3388	22.41135	14.53552	1.192308	1.970443	29.62074	5.888224	4.078526	2.829343	2.219335	1.245318	1.635514	1.354034	0.905367	0.251748	0.606481	0.505498	0.508872	0.4875	8.014836	53.12286
Meta-Basalt, Amphibolite (Jeddah terrane)	8.333333	12.51724	24.85656	3.439716	2.04918	0.48495	0.492611	7.116671	2.42515	2.028846	4.714789	1.746362	0.662921	0.864486	1.410828	1.245763	0.933942	0.930556	0.845361	0.872624	0.7375	2.324996	51.25594
ADSZ Rocks	33.7963	66.25862	94.69262	59.80496	25.2459	1.463211	1.477833	33.8138	9.678144	5.401442	2.247359	2.785863	1.758427	2.336449	1.437102	0.959746	0.220842	0.635417	0.521649	0.614068	0.61875	8.796157	64.71564
Granitoid Rock (Asir Terrane)	34.44444	73.51724	112.1585	77.49409	24.42623	1.694537	1.642036	33.30089	10.56886	6.346154	3.090376	2.588358	2.26779	2.593458	1.17569	0.672316	0.227023	0.393519	0.27732	0.228771	0.229167	27.74025	66.18825
Folded silisic dike-AD damm drag fold	7.037037	39.17241	54.31694	49.17258	38.4153	3.991081	3.612479	29.2617	10.43912	8.810897	0.488028	6.039501	3.640449	5.560748	4.855626	0.920904	0.074176	3.740741	3.484536	4.38403	4.25	2.009771	13.60958
Folded basaltic dike-AD damm drag fold	24.12037	55.2069	81.34477	54.58333	23.59631	2.238712	2.124384	28.27915	9.03256	5.932692	2.610211	3.214657	2.235253	2.908879	2.041003	0.940148	0.373408	1.238715	1.093428	1.269487	1.220313	4.6733	36.33552
Eocene-Miocene Ad Damm Dikes complex	6.17284	3.885057	15.27322	7.163121	4.863388	2.552954	2.298851	2.513275	3.143713	2.451923	2.455399	1.878032	1.318352	1.557632	1.532909	1.398305	1.213787	1.199074	1.132646	1.136882	1.058333	2.156708	5.982569
Southern basalt flow	2.222222	2.482759	18.52459	3.971631	3.442623	1.003344	0.985222	2.231172	2.065868	1.576923	3.492958	1.195426	0.94382	1.121495	1.038217	1.016949	0.768732	0.763889	0.717526	0.684411	0.75	2.30406	18.46284

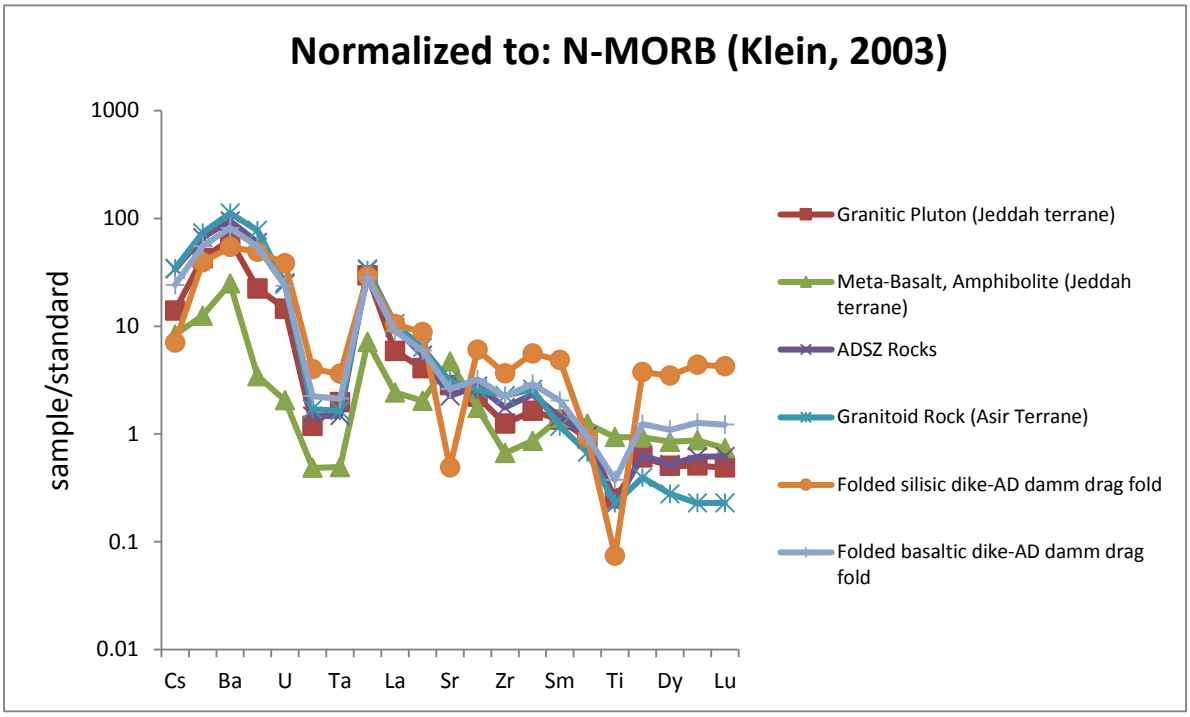

Figure 2.31 N-MORB (Klein, 2003) Averaged spider element diagram for Jeddah terrane (granitic plutons, silicic & basaltic folded dikes, and amphibolite/ meta-basalt), Asir terrane, ADSZ rocks, Eocene-Miocene basaltic dikes, and southern basaltic flow.

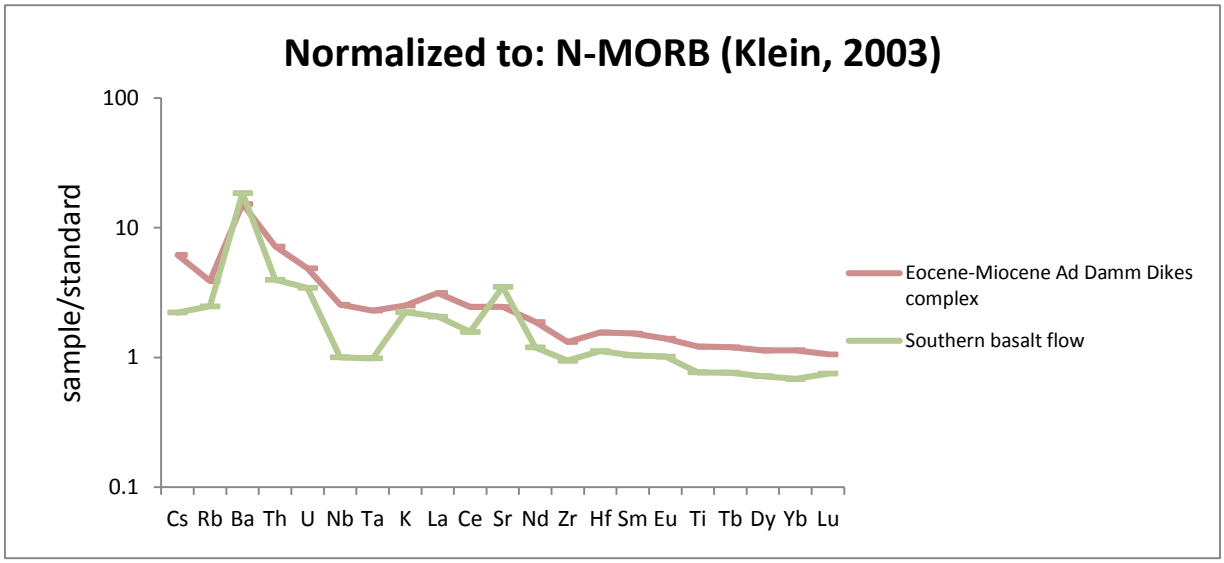

Figure 2.32 N-MORB (Klein, 2003) incompatible element diagram for Eocene-Miocene basaltic dikes and basaltic flow.

3.4.3 Tectonic Discrimination Diagrams

Geochemical tectonic discrimination diagrams are used to distinguish between magmas that form in different tectonic environments (Rollinson, 1993). Elements utilized in discrimination diagrams are include: (Ti, Zr, Y, V, Nb, and Sr). These elements have huge impact on classifying basalts that form from different tectonic setting. Also important to consider in the tectonic discrimination diagrams is the use of immobile trace elements or HFS elements(Ti, Zr, Y,V, Nb, and Sr), which are not influenced significantly by hydrothermal activities and are stable under circumstances such as weathering and up to intermediate grades of metamorphism. In general, basaltic rock units are used to distinguish between oceans ridges and volcanic arc, while granitic rock unites are used for collision zones discrimination (Rollinson, 1993).

In this project we have picked Ti-V diagram to differentiate between the basaltic units that generate from volcanic arc, tholeiites, MORB and alklie basaltic composition (because more data are available compared to other elements). The diagram (Shervais, 1982) is constructed based on the ratio of (Ti/V) and subdivided basaltic samples into three groups. MORB, the first group, has Ti/V ratio ranging between 50-20. Arc tholeiites group, second group, include samples of Ti/V ratio ranging between 10- 20. Third group, Ocean Island and alkalis basalt is bounded by Ti/V ratio from 50 to 100. V vs. Ti diagram (Figure 2.31) indicates the Eocene-Miocene Ad dam dikes complex, and southern basalt flow are classified as MORB with composition of low- medium K calc alkaline. However, the folded basaltic dikes of Jeddah terrane is defined as alkali basalt due to high potassium concentration, which is well correlated with previous classification of sub-alkalic rocks using SiO2 vs. K2O (La Maitre et al., 1989).

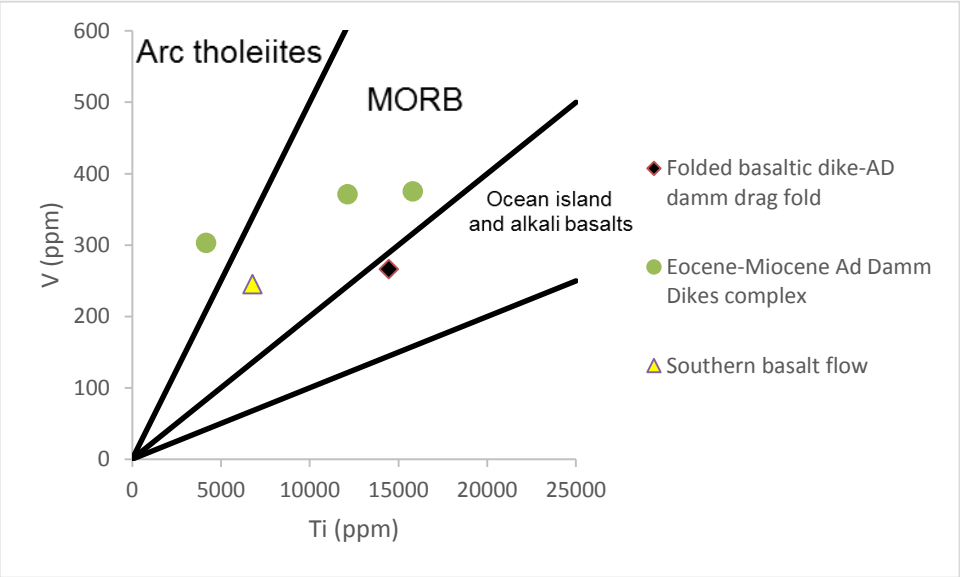

Figure 2.33 Ti/V discrimination diagram for basaltic units of study area (Shervais, 1982).

In addition to the basaltic tectonic discrimination diagram, Ta-Yb and Rb vs. (Yb+Ta) diagrams Pearce et al. (1984) were used to distinguish between different types of granites. Commonly, granitic rocks are divided, on the basis of their location in to volcanic-arc, ocean ridge, within plate, and collision types. The trace elements most useful in discriminating granitic units are (Y, Yb, Rb, Ba, K, Nb, Ta, Ce, Sm, Zr, and Hf). Many studies have shown Rb-(Yb+Ta) and Ta to Yb ratios can be used in classifying the tectonic origin granitic units, and thus they have been used in our study.

Both Ta-Yb and Rb- (Yb+Ta) discrimination diagrams (Pearce et al., 1984) display a similar pattern, where all intrusive units clustered within volcanic arc granites except for the folded silicic dikes, which falls within the field of within plate granite. However, the folded silicic dike unit also as arc related signature such as the large negative Nb-Ta anomaly as shown above in the spider diagram.

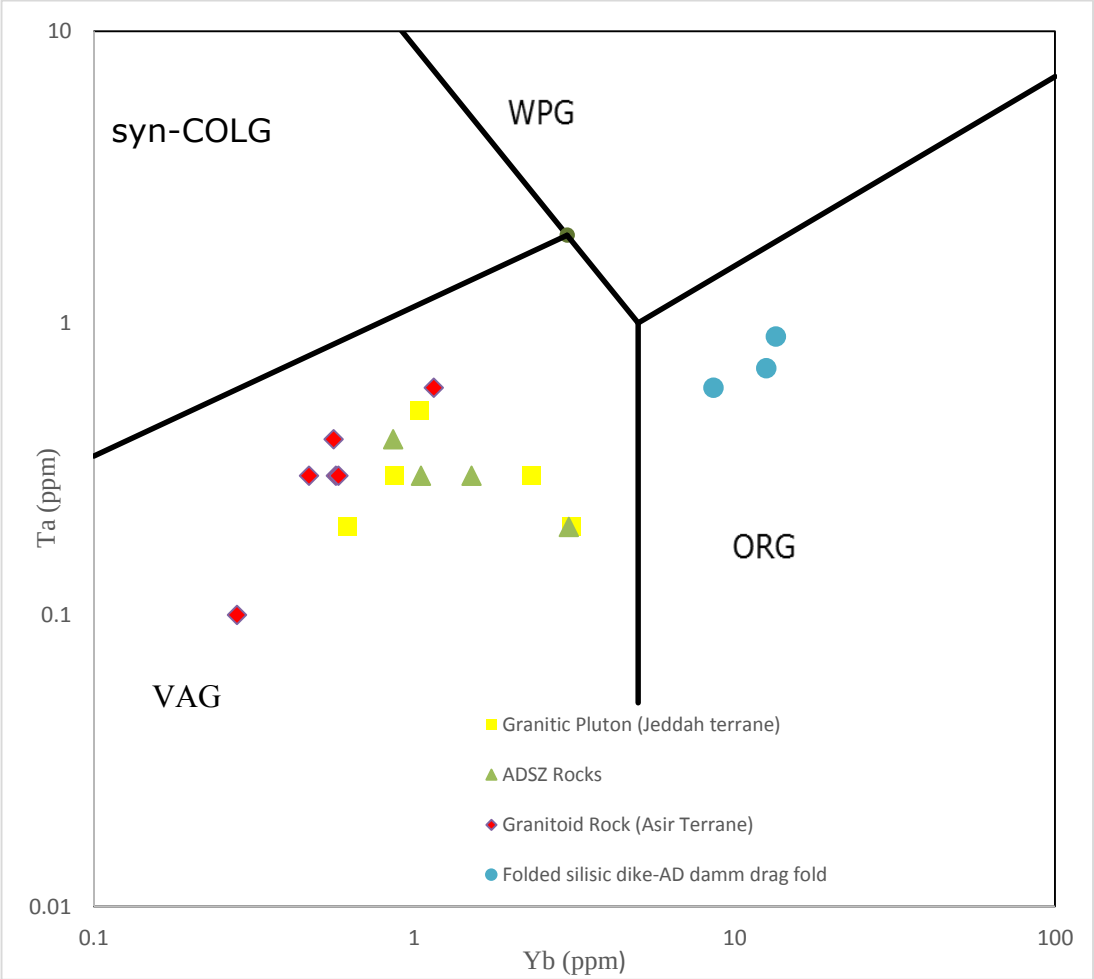

Figure 2.34 Ta-Yb discrimination diagram for granitic rock units in the study area (Pearce et al., 1984).

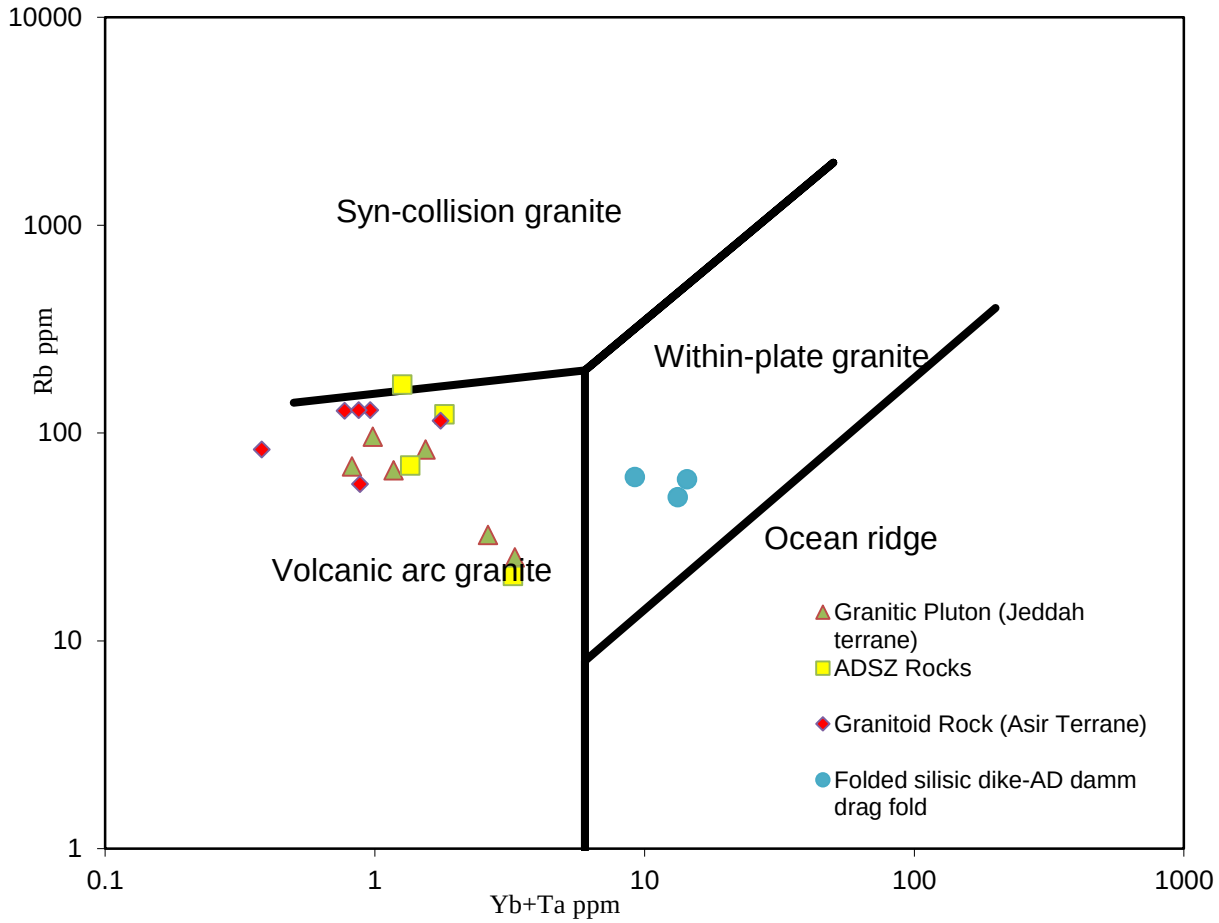

Figure 2.35 Rb- (Yb+Ta) discrimination diagram for granitic rock units in the study area (Pearce et al., 1984).

CHAPTER 3

DISCUSSION

Overall, findings represented here support the hypothesis that the ADSZ is a Neoproterozoic structure. However, the ADSZ still influences the neotectonic evolution of Red Sea margin via inherited differences in crustal characteristics between the Jeddah and Asir terranes. The seismicity recorded along and around the Ad Damm area as well as crustal topographic variation between the Asir and Jeddah terranes, imply the area is tectonically active, and yet cross-cutting relationships of rift related dikes with respect to the Ad Damm shear zone suggest that it is a pre-Cenozoic structure.

The recent seismicity surrounding the ADSZ is a significant evidence of reactivation of old Neoproterozoic structure. According to Al- Saud (2008), the area of study is influenced by NE-SW lateral movement. The distribution of focal mechanism solutions illustrates a component of right-lateral seismicity along the ADSZ (Figure 3.1). Moreover, the extension of seismicity around ADSZ matches with direction of structural lineament using aeromagnetic data analysis, which also support the reactivation of ADSZ (Figure 2.35). Slip vectors data coupled from the focal mechanism solution display the predicted motion of ADSZ to N30±05ºE and Makkah north of (AD Damm area) to N30±10ºE. To sum up, the presented model (Al Saud, 2008) displays active movement of Arabian plate in general and Makkah region in particular toward NNW, which is related to rifting system of Red Sea. However, observations presented here show essentially no observations of Ad Damm shear zone surface displacement or any sort of low temperature brittle deformation features (e.g. fault gouge) associated with active faulting. Therefore, the interpretive question is how can such conflicting data sets be reconciled?

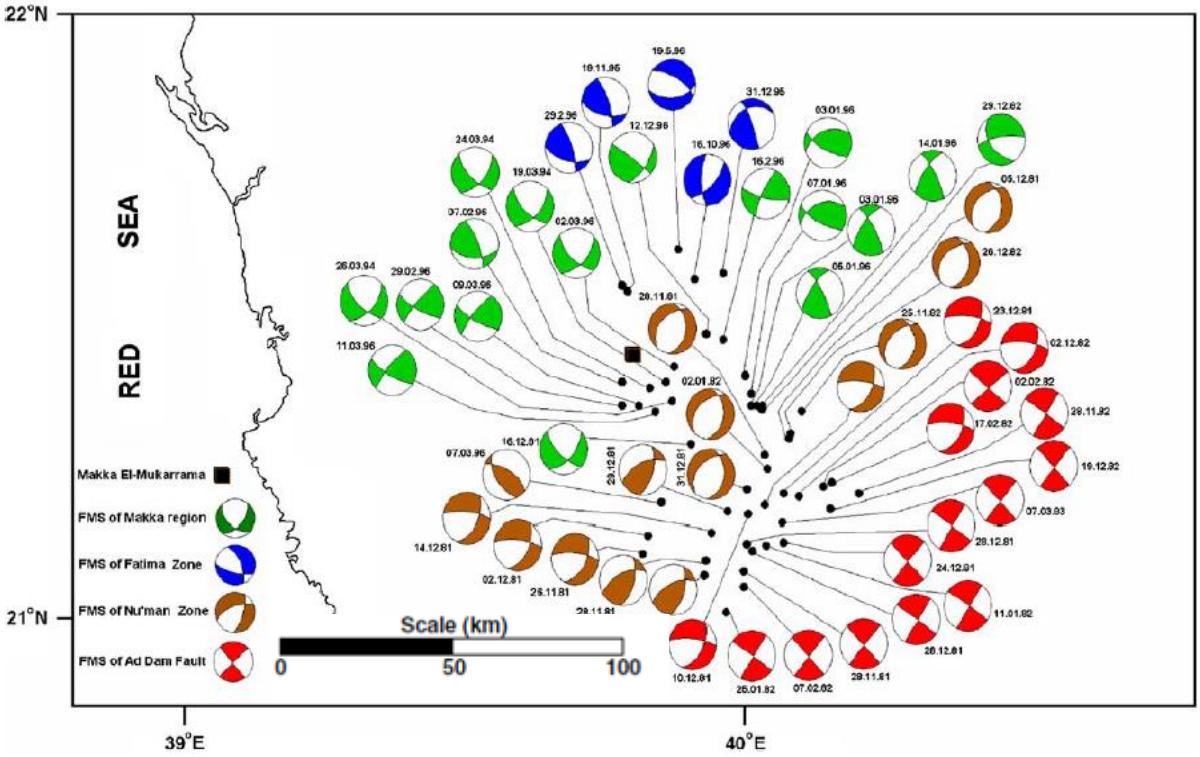

Figure 3.1 Displays focal mechanism solutions in Ad Damm area (Al- Saud, 2008).

Al-Damegh et al. (2005), represents seismically based estimates of crustal thickness in the Arabian plate (Figure 3.2). Average crustal thickness along the western margin of the Arabian plate ranges between 23 (along the costal line) to 25 km in Gulf of Aqaba. While the average thickness of central part of the Arabian shield is about 40 km (Al-Damegh et al., 2005). Offshore, in the Red sea crustal thickness thins to 14.5 km thick, and presumably to zero at the ridge axis along which new oceanic crust is being created. In general, Arabian shield- crustal thicknesses are greater in the southern half of the Peninsula (30-35 km vs 40-45 km), and this change is located near the latitude of the Ad Damm Shear zone. However, greatest crustal thicknesses range from 46 km in Arabian platform to 51 km in the Arabia Persian gulf (Al-Amri, 2000). Crustal thickness differences also exist between Jeddah and Asir terranes, in which

Asir terrane is thicker of about 5-8 km. This observation was carried out using seismic receiver functions (Al-Damegh et al., 2005) to image and estimate Moho's depth.

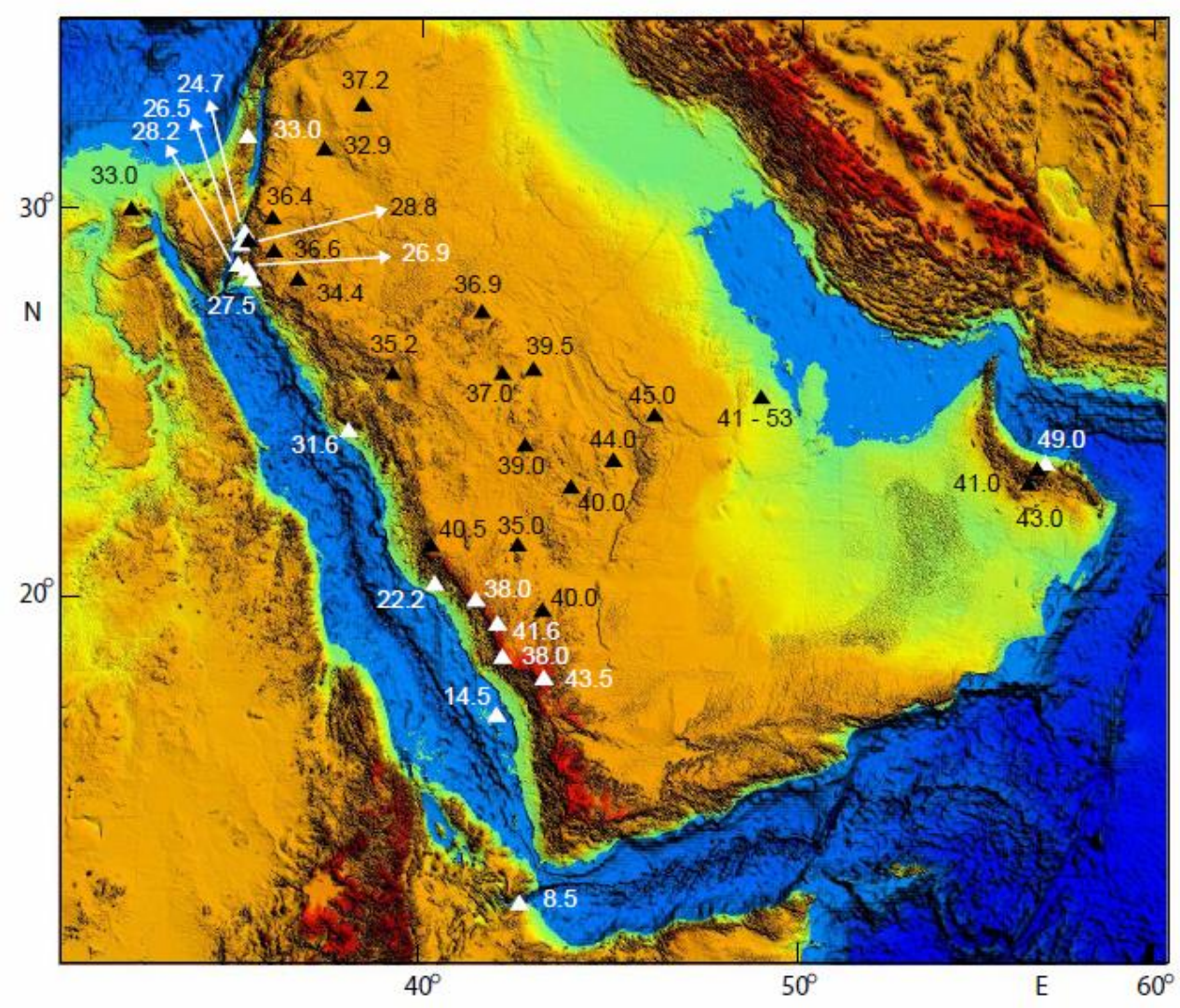

Figure 3.2 Displays variations in the crustal thickness observed by 36 teleseismic stations around the Arabian shield (Al-Damegh et al., 2005).

In addition, the Mantle and Collins (2008), method of estimating arc crustal thicknesses using trace element geochemical data was applied to determine the difference in the crustal

thickness between the Asir and Jeddah terranes. In general, the ratio of LREE to HREE increases with increase arc crustal thickness due to the deeper crystallization of minerals such as garnet and hornblende that preferentially absorb HREE (Figure 2.29). Mantle and Collins (2008) calibrated this relationship using the Ce (as LREE) and Y (as HREE approx.) ratio. And therefore, arc Moho depth can be calculated by using this equation:

$$\text{Arc Moho depth (km)} = \ln((Ce/Y)/0.3029) / 0.0554$$

Our finding suggest that the Jeddah terrane has thickness of approximately 30 km and the Asir terrane is approximately 8 km thicker, which is well-correlated with Al- Amri and Gharib (2000) and Al- Damegh et al. (2005). The crustal thickness variations and topographic differences suggest an uplifting of Asir terrane during opening of Red Sea (Figure 3.3)). Such crustal thickness variations will produce a significant isostatic effect and therefore the inherited crustal characteristics of the Jeddah and Asir terranes may explain the observed difference in elevation across the ADSZ (Figure 3.3).

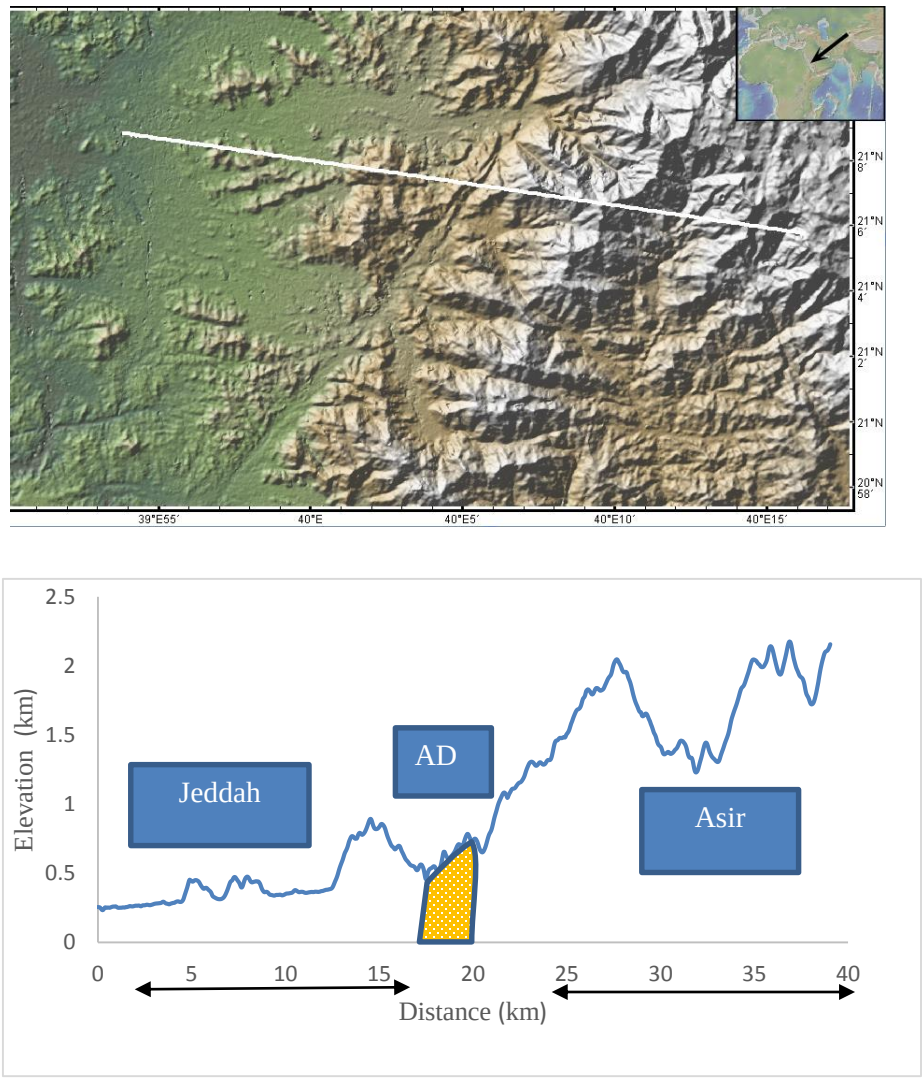

Figure 3.3 Elevation profile across Jeddah, ADSZ, and Asir terranes, using Geomap App.

CHAPTER 4

CONCLUSION

The main objective of this project is to better understand the opening of the Red Sea rift and to place constraints on the tectonic and structural evolution of the western Saudi Arabian margin. More specifically, the study aims to determine whether or not the Ad Damm Shear Zone (ADSZ) was solely a Neoproterozoic structure or if it has been reactivated during the Cenozoic. The study area is dominated by ADSZ which strikes NE-SW, and forms the boundary between Jeddah and Asir terrane.

Previous geochronological works have shown that Arabian plate is shaped by amalgamation of nine terranes (Johnson, 1997). Older terranes include Jeddah (870- 740 Ma; KrÖner et al., 1993) and Asir Terrane (850- 750 Ma; Johnson and Woldehaimaot, 2003). The age of ADSZ granitic rocks was also determined (542± 23) using a whole rock multi-sample Rb-Sr radiometric dating technique. However, Johnson (2006) indicates that the calculated age might be related to the cooling age of rock- forming minerals, instead of the recrystallization age during the shearing event.

Tectonically, deformation of the shear zone on the other flank of Red Sea (Nubian shield) is similar and compatible with the deformation in the Ad Damm Shear Zone, which indicates that ADSZ took place during Neoproterozoic.

However, geophysical data illustrates a well-developed linear magnetic anomalies in the southern part of Red (South of ADSZ). However, linear magnetic anomalies are not present in the northern segment. In addition to that, recent studies observe and measure the seismicity along ADSZ area (Al-Saud, 2008), which in turn, suggests reactivation along ADZS.

In order to evaluate these questions regarding the Ad Damm Shear Zone, field mapping coupled

with satellite image processing (ASTER, , Landsat-8, Mr-SID, and SPOT-5), petrological and microstructural studies, and whole rock geochemistry were carried out.

Our findings can be summarized into the following points:

1- Large-scale synform drag fold, located along the northern part of ADSZ, where Jeddah rock units are folded and intruded by Eocene-Miocene basaltic dikes at high angle.

2- Petrographic and microstructure analyses indicate gradual evolution of sub-grains with undulose extinction near to the both sides of ADSZ, while the mylonitic rocks of ADSZ shows dynamic recrystallization and grain size reduction suggesting high-temperature recrystallization.

3- Major elements classification for plutonic and volcanic rocks interpret the majority of plutonic rocks as high K calc-alkaline. Whereas, the Eocene-Micocene basaltic dikes are relatively defined as tholiietic composition.

4- Normalized multi-element diagram specifies Jeddah, Asir terranes, and ADSZ rocks have similar REE pattern, and are characterized by an arc- related signature. ADSZ is fomed associated with amalgamation of Jeddah and asir terranes. In contrast, Eocen-Miocene Basaltic dikes and southern basaltic flow are represented by rift- related signature, and with development of Red Sea rift system.

5- Crustal thickness differences between Asir and Jeddah terranes make ADSZ act as crustal boundary, and current seismicity long ADSZ, still influence the neotectonics of the Red Sea.

REFERENCES

Al-Amri, A. M., & Gharib, A. A. (2000). Lithospheric seismic structure of the eastern region of the Arabian Peninsula. *Journal of Geodynamics*, *29*(1), 125-139.

Al-Saud, M. M. (2008). Seismic characteristics and kinematic models of Makkah and central Red Sea regions. *Arabian Journal of Geosciences*, *1*(1), 49-61.

Al-Saud, M. M (2008). Structural mapping from high resolution aeromagnetic data in west central Arabian Shield, Saudi Arabia using normalized derivatives. *Arabian Journal of Geosciences*1.2: 129-136.

Al-Damegh, K., Sandvol, E., & Barazangi, M. (2005). Crustal structure of the Arabian plate: new constraints from the analysis of teleseismic receiver functions. Earth and Planetary Science Letters, 231(3), 177-196.

Ali, K.A., Stern, R.J., Manton, W.I., Kimura, J.I., Whitehouse, M.J., Mukherjee, S.K., Johnson, P.R., Griffin, W.R., 2010. Geochemical, U–Pb zircon, and Nd isotope investigations of the Neoproterozoic Ghawjah Metavolcanic rocks, Northwestern Saudi Arabia. Lithos 120, 379–393

Bohannon RG, Naeser CW, Schmidt DL, Zimmermann RA (1989) The timing of uplift, volcanism, and rifting peripheral to the Red Sea: a case for passive rifting? J Geophys Res Solid Earth 94(B2):1683– 1701. doi:10.1029/JB094iB02p01683

Camp, V. E., Roobol, M. J., & Hooper, P. R. (1991). The Arabian continental alkali basalt province: Part II. Evolution of Harrats Khaybar, Ithnayn, and Kura, Kingdom of Saudi Arabia. *Geological Society of America Bulletin*, *103*(3), 363-391.

Coleman, R.G. (1993). Geologic Evolution of the Red Sea. Oxford monographs on geology and geophysics. Oxford University Press. P. 77-99.

Camp VE, Roobol MJ (1992 a) Upwelling asthenosphere beneath western Arabia and its regional implications. J Geophys Res 97:15255– 15271

Dong, H. (2003). Semi-automated extraction of urban road networks by geometric analysis of IKONOS imagery (Doctoral dissertation, East China University of Science & Technology, China, 1994).

Fleck, R.J., Hadley, D.G., (1982). Ages and Strontium Initial Ratios of Plutonic Rocks in a Transect of the Arabian Shield. Saudi Arabian Deputy Ministry for Mineral Resources Open-File, Report USGS-OF-03-38, 43 p.

Hamimi, Zakaria, et al. (2014). "Neoproterozoic structural evolution of the NE-trending Ad-

Damm Shear Zone, Arabian Shield, Saudi Arabia." *Journal of African Earth Sciences* 99: 51-63.

Hartmann, L. A., Santos, J. O. S., Bossi, J., Campal, N., Schipilov, A., & McNaughton, N. J. (2002). Zircon and titanite U–Pb SHRIMP geochronology of Neoproterozoic felsic magmatism on the eastern border of the Rio de la Plata Craton, Uruguay. Journal of South American Earth Sciences, 15(2), 229-236.

Johnson, P.R., 2006. Explanatory Notes to the Map of Proterozoic Geology of Western Saudi Arabia. Saudi Geological Survey Technical, Report SGS-TR-2006- 4: 62

Johnson P (1997) Tectonic map of Saudi Arabia and adjacent areas. Ministry for Mineral Resources, Technical report USGS-TR-98-3, scale 1:40,000,000.

Johnson PR, Woldehaimanot B (2003) Development of the Arabian– Nubian Shield: perspectives on accretion and deformation in the northern East African Orogen and the assembly of Gondwana. In:

Yoshida M, Windley B, Dasgupta S (eds) Proterozoic East Gondwana: supercontinent assembly and breakup. Geological Society, London, Special Publications. Geological Society of London, London, pp 289–325

Kro¨ner, A., 1993. The Pan African belt of northeastern and Eastern Africa, Madagascar, southern India, Sri Lanka and East Antarctica: terrane amalgamation during the formation of the Gondwana supercontinent. In: Thorweihe, U., Schandelmeier, H. (Eds.), Geoscientific Research in Northeast Africa. Balkema, Rotterdam, pp. 3–9.

Ludwig, K. R. (2000). Decay constant errors in U–Pb concordia-intercept ages.Chemical Geology, 166(3), 315-318.

Lazar, M., Ben-Avraham, Z., & Garfunkel, Z. (2012). The Red Sea–New insights from recent geophysical studies and the connection to the Dead Sea fault. *Journal of African Earth Sciences*, *68*, 96-110.

Pour, A. B., & Hashim, M. (2012). The application of ASTER remote sensing data to porphyry copper and epithermal gold deposits. *Ore Geology Reviews*,*44*, 1-9.

Peyton, S. L., & Carrapa, B. (2013). An overview of low-temperature thermochronology in the Rocky Mountains and its application to petroleum system analysis. Application of Structure Methods to Rocky Mountain Hydrocarbon Exploration and Development, 65, 37-70.

Pasqualini, V., Pergent-Martini, C., Pergent, G., Agreil, M., Skoufas, G., Sourbes, L., & Tsirika, A. (2005). Use of SPOT 5 for mapping seagrasses: An application to Posidonia oceanica. *Remote Sensing of Environment*, *94*(1), 39-45.

Roobol M, Kadi K. (2008) Cenozoic Faulting System Central-West Saudi Arabia. Saudi

Geological Survey. Jeddah. Saudi Arabia, 12 pp.

Sabins, F. F. (1999). Remote sensing for mineral exploration. Ore Geology Reviews, 14(3), 157-183.

Shand, M. (2002). Mapping and imaging Africa on the Internet.INTERNATIONAL ARCHIVES OF PHOTOGRAMMETRY AND REMOTE SENSING, 34(6/W6), 210-217.

Stern, R. J., & Johnson, P. (2010). Continental lithosphere of the Arabian Plate: a geologic, petrologic, and geophysical synthesis. Earth-Science Reviews,101(1), 29-67.

Stoeser, D.B., Stacey, J.S., 1988. Evolution, U–Pb geochronology and isotope geology of the Pan-African Nabitah orogenic belt of the Saudi Arabian Shield. In: El- Gaby, S., Greiling, R.O. (Eds.), The Pan-African Belt of Northeast Africa and Adjacent Areas: Braunschweig/Wiesbaden. Vieweg and John, pp. 227–288 A

Schmid, S. M., & Kissling, E. (2000). The arc of the western Alps in the light of geophysical data on deep crustal structure. *Tectonics*, *19*(1), 62-85.

BIOGRAPHICAL SKETCH

Abdulaziz Samkari is a geoscientist and a graduate student at Florida State University, Tallahassee, FL. He received his B.S. in engineering geology from King Abdulaziz University in 2008 and worked with Saudi Aramco for three years before eventually becoming a teaching assistant at King Abdulaziz University in 2011. For the past three years with Saudi Aramco, he worked as a field geologist in Saudi Arabia and as a wire- line field engineer in Egypt, Russia, Indonesia, the United Arab Emirates, and Saudi Arabia. While he was drawn to the generous salary of the oil sector, he changed his interest after discovering the joys of teaching geology. Abdulaziz is currently specializing in neotectonics and the recent structures associated with rifting of the Red Sea. His long- term goal is to gain a better understanding of the rifting system and the geologic hazards associated with in Saudi Arabia. His current research is funded by King Abdulaziz University and the Ministry of Higher Education, Saudi Arabia.